



## ESA Climate Change Initiative (CCI+)

### Essential Climate Variable (ECV)

### Greenland\_Ice\_Sheet\_cci+ (GIS\_cci+)

## Product Validation and Intercomparison Report (PVIR)

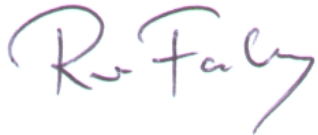
Prime & Science Lead: René Forsberg  
DTU Space, Copenhagen, Denmark  
[rf@space.dtu.dk](mailto:rf@space.dtu.dk)

Technical Officer: Marcus Engdahl  
ESA ESRI, Frascati, Italy  
[Marcus.Engdahl@esa.int](mailto:Marcus.Engdahl@esa.int)

Consortium:  
Asiaq Greenland Survey (ASIAQ)  
DTU-Space, Department of Geodynamics (DTU-S)  
DTU-Space, Department of Microwaves and Remote Sensing (DTU-N)  
Danish Meteorological Institute (DMI)  
ENVIRONMENTAL Earth Observation IT GmbH (ENVEO)  
Science [&] Technology AS (S&T)  
Technische Universität Dresden (TUDr)  
The Geological Survey of Denmark and Greenland (GEUS)  
The Niels Bohr Institute (NBI)  
University of Leeds, School of Earth and Environment (UL)



## Signatures page

Prepared by	Anne Solgaard		Date: 2020.10.09
Issued by	Daniele Fantin, Project Manager, S&T		Date: 2020.10.14
Checked by	Rene' Forsberg Science Leader, DTU-S		Date: 2020.10.14
Approved by	Marcus Engdahl ESA Technical Officer		Date:

## Table of Contents

<b>Signatures page</b> .....	<b>2</b>
<b>Table of Contents</b> .....	<b>3</b>
<b>Change Log</b> .....	<b>5</b>
<b>Acronyms and Abbreviations</b> .....	<b>6</b>
<b>1 Introduction</b> .....	<b>8</b>
1.1 Purpose and Scope .....	8
1.2 Document Structure .....	8
1.3 Applicable and Reference Documents.....	8
<b>2 Surface elevation change (SEC)</b> .....	<b>10</b>
2.1 Sources and selection of independent validation data .....	10
2.1.1 Validation data errors and biases .....	10
2.2 Validation procedure .....	11
2.3 Validation procedure outcome .....	12
2.4 Recommendations for products improvement.....	12
<b>3 Ice Velocity (IV)</b> .....	<b>13</b>
3.2 Radar IV .....	13
3.2.1 Sources and selection of independent validation data .....	13
3.2.2 Validation procedure.....	14
3.2.3 Validation procedure outcome.....	15
3.2.4 Recommendations for products improvement .....	19
1.3.1 Acknowledgments of data contributors for IV validation .....	20
3.3 Optical IV .....	21
3.3.1 Sources and selection of independent validation data .....	21
3.3.2 Validation procedure.....	21
3.3.3 Validation procedure Outcome .....	21
23	
24	
3.3.4 Recommendations for products improvement .....	24
<b>4 Gravimetry Mass Balance (GMB)</b> .....	<b>25</b>
4.1 (Inter-) comparison procedure .....	25
4.2 (Inter-) comparison procedure outcome .....	25
4.3 Recommendations for products improvement.....	28
<b>5 Mass Flow Rate and Ice Discharge (MFID)</b> .....	<b>30</b>
5.1 Sources and selection of independent validation data.....	30
5.2 Validation procedure .....	30
5.3 Validation procedure outcome .....	30
5.4 Recommendations for products improvement.....	30
<b>6 Supraglacial Lakes</b> .....	<b>40</b>
6.1 Sources and selection of independent validation data.....	40
6.2 Validation procedure .....	41
6.3 Validation procedure outcome .....	41
6.4 Recommendations for products improvement.....	42



greenland  
ice sheet  
cci

Greenland\_Ice\_Sheet\_cci+  
Product Validation and Intercomparison Report  
(PVIR) for CCI+ Phase 1

Reference: ST-DTU-ESA-GISCCI+-PMP-001  
Version : 1.0 page  
Date : 14 Oct 2020 4/45

**7 References ..... 43**



## Change Log

Issue	Author	Affected Section	Change	Status
0.5	S&T	All	Document Creation	
1.0	GEUS + All	All	Input on ECV validation and intercomparison	

## Acronyms and Abbreviations

Acronyms	Explanation
<b>ATBD</b>	Algorithm Theoretical Basis Document
<b>C3S</b>	Copernicus Climate Change Service
<b>CCI</b>	Climate Change Initiative
<b>CFL</b>	Calving Front Location
<b>CS2</b>	CryoSat-2
<b>CSR</b>	Center for Space Research, University of Austin
<b>DEM</b>	Digital Elevation Model
<b>DInSAR</b>	Differential Interferometric Synthetic Aperture Radar
<b>DMI</b>	Danish Meteorological Institute
<b>DTU-N</b>	DTU Microwaves and Remote Sensing Group
<b>DTU-S</b>	DTU Geodynamics Group
<b>E3UB</b>	End-to-End ECV Uncertainty Budget
<b>ECV</b>	Essential Climate Variable
<b>ENU</b>	East North Up
<b>ENVEO</b>	ENVironmental Earth Observation GmbH
<b>EO</b>	Earth Observation
<b>ESA</b>	European Space Agency
<b>GCOS</b>	Global Climate Observation System
<b>GCP</b>	Ground Control Point
<b>GEUS</b>	Geological Survey of Denmark and Greenland
<b>GFZ</b>	Deutsche GeoForschungsZentrum
<b>GIA</b>	Glacial Isostatic Adjustment
<b>GIS</b>	Greenland Ice Sheet
<b>GLL</b>	Grounding Line Location
<b>GMB</b>	Gravimetry Mass Balance
<b>GRACE(-FO)</b>	The Gravity Recovery and Climate Experiment (Follow On)
<b>IMBIE</b>	Ice Sheet Mass Balance Inter-Comparison Exercise
<b>InSAR</b>	Interferometric Synthetic Aperture Radar
<b>IPP</b>	Interferometric Post-Processing
<b>IV</b>	Ice Velocity
<b>JPL</b>	NASA Jet Propulsion Laboratory
<b>MAI</b>	Multiple Aperture Interferometry
<b>MEaSURES</b>	Making Earth System Data Records for Use in Research
<b>MFID</b>	Mass Flow Rate and Ice Discharge
<b>NBI</b>	Niels Bohr Institute, University of Copenhagen
<b>NEGIS</b>	North East Greenland Ice Stream
<b>PROMICE</b>	Danish Program for Monitoring of the Greenland Ice Sheet
<b>RA</b>	Radar Altimetry
<b>RMS</b>	Root Mean Square
<b>S&amp;T</b>	Science and Technology AS



<b>S2</b>	Sentinel-2
<b>SAR</b>	Synthetic Aperture Radar
<b>SEC</b>	Surface Elevation Change
<b>SLR</b>	Satellite Laser Ranging
<b>SMB</b>	Surface Mass Balance
<b>SOW</b>	Statement of Work
<b>TEC</b>	Total Electron Content
<b>TOA</b>	Top of Atmosphere
<b>TPROP</b>	Technical Proposal
<b>TUDr</b>	Technische Universität Dresden
<b>UL</b>	University of Leeds
<b>URD</b>	User Requirement Document

# 1 Introduction

## 1.1 Purpose and Scope

This document contains the Product Validation and Inter-comparison Report (PVIR) for the Greenland\_Ice\_Sheet\_cci+ (GIS\_cci+) project for CCI+ Phase 1, in accordance with contract and SoW [AD1 and AD2].

This document describes the results of the validation and intercomparison activities described in the Product Validation Plan for the Greenland\_Ice\_Sheet\_cci (GIS\_cci) project for CCI+ Phase 1 [RD1] for the four types of data products:

- Surface elevation Change;
- Ice Velocity;
- Gravimetry Mass Balance;
- Mass Flow Rate and Ice Discharge;

As well as the research object:

- Supraglacial Lakes

The results of these activities will provide input for reviewing the product specifications and algorithms in order to provide feedback for Cycle 2 products.

## 1.2 Document Structure

This document is structured as follows:

Chapter 1 contains an introduction to the document.

Chapter 2 – 6: A chapter for each ECV and the research object. The IV chapter is split in radar IV and optical IV. Each chapter contains section describing the validation data sets, validation procedure and outcome and recommendations for product improvement.

Chapter 7 contains a reference list.

## 1.3 Applicable and Reference Documents

**Table 1.1: List of Applicable Documents**

No	Doc. Id	Doc. Title	Date	Issue/ Revision/ Version
AD1	ESA/Contract No. 4000126023/19/I-NB, and its Appendix 1	CCI+ PHASE 1 - NEW R&D ON CCI ECVS, for Greenland_Ice Sheet_cci	2019.04.01	
AD2	ESA-CCI-EOPS-PRGM-SOW-18-0118 Appendix 2 to contract.	Climate Change Initiative Extension (CCI+) Phase 1, New R&D on CCI ECVs Statement of Work	2018.05.31	Issue 1 Revision 6
AD3	ST-DTU-ESA-GISCCI-PVP-001	Product Validation Plan for the Ice_Sheets_cci project of ESA's Climate Change Initiative	2012.08.21	
AD4	ST-DTU-ESA-GISCCI-PVIR-001	Greenland_Ice_Sheet_cci Product Validation and Intercomparison Report	2018.07.25	
AD5	ST-DTU-ESA-GISCCI-PSD-001	.Product Specification Document for the Ice_Sheets_cci project of ESA's Climate Change Initiative	2016.06.20	Version 2.2

 <b>greenland ice sheet cci</b>	Greenland_Ice_Sheet_cci+ Product Validation and Intercomparison Report (PVIR) for CCI+ Phase 1	Reference: ST-DTU-ESA-GISCCI+-PMP-001 Version : 1.0 page Date : 14 Oct 2020 9/45
--	--	--

**Table 1.2: List of Reference Documents**

No	Doc. Id	Doc. Title	Date	Issue/ Revision/ Version
RD1	ST-DTU-ESA-GISCCI+-PVP-001	Greenland_Ice_Sheet_cci+ Product Validation Plan	2019.07.02	
RD2	ST-DTU-ESA-GISCCI+-ATBD-001	Greenland_Ice_Sheet_cci+ Algorithm Theoretical Basis Document (ATBD) for CCI+ Phase 1	2020.02.02	

**Note:** If not provided, the reference applies to the latest released Issue/Revision/Version

## 2 Surface elevation change (SEC)

The validation strategies are described in section 6.1 of the "Product Validation Plan for the Ice\_Sheets\_cci project of ESA's Climate Change Initiative" [AD3], however the described round robin will be omitted. Hence, the main validation efforts will focus on:

- Comparison of temporally consistent airborne elevation changes with satellite altimeter elevation changes.
- Comparison of elevation changes derived from different sensors (e.g. radar vs. laser).

The SEC validation will be based upon the following metrics:

- RMSE (with respect to independent validation data)
- Temporal/spatial coverage and density of observations.

This chapter gives a complete report of the activities carried out to assess the quality of the SEC products. In section 2.1 the sources of independent validation data considered for the SEC product validation, can be found, section 2.2 describes the validation procedure undertaken for the final SEC product, section 2.3 gives the results of the performed validation, before the recommendation for future improvements are described in section 2.4.

### 2.1 Sources and selection of independent validation data

The main source of validation data for the SEC-product are elevation change derived from repeat airborne laser scanning. Due to the significantly smaller horizontal and vertical errors associated with laser data compared to radar data (Brenner et al., 2007), the SEC trends are validated against elevation change trends derived from airborne laser-scanner data after being averaged at similar grid resolution as the SEC product.

Here, two different observational platforms and data products are used:

1. NASA's Operation IceBridge (Krabill, 2014) Airborne Topographic Mapper (ATM). The ATM data are acquired seasonally in the months April to June, and on a nearly yearly basis starting in 1993. The ATM instrument is mounted on-board an aircraft, usually the NASA DC-8 or P3-B, and typically flown at an altitude of 450 m. Given a 30-degree swath width, the laser pulses illuminate an approximately 250 m wide path on the ground. Each pulse has a footprint diameter of 1 to 3 m. The elevation change trends used in the validation are generated from the IceBridge ATM L1B Elevation and Return Strength (version 2) product (Krabill, 2010), and the surface elevation change is available at the National Snow and Ice Data center as a Level-4 data product.
2. DTU airborne laser scanning (ALS) conducted as part of the Programme for Monitoring of the Greenland Ice Sheet (PROMICE) or ESA's CryoSat Validation Experiment (CryoVEx) campaigns (Blair and Hofton, 2012; Geological Survey of Denmark and Greenland, 2015; Sørensen et al., 2018; Skourup, 2011). The DTU ALS system measures surface elevation measurements from scanning the surface in an approximately 200m wide swath, and surface elevation change have been derived from all available repeat flight paths. In contrast to the ATM dataset the ALS data also contain surface elevation change records from autumn campaigns.

An advantage of using airborne campaigns is that they most often are targeted at areas of the ice sheet which undergoes significant surface changes, both in time and space and thereby are multiple repeats available over especially the ice margin, where the largest SEC occurs and the radar altimeter observations is most challenged. Additionally, the long time series of airborne observations also ensures that we have a representative sampling over the more stable interior of the ice sheet.

#### 2.1.1 Validation data errors and biases

Errors in airborne laser scanning arise from several sources, such as errors in the pitch, roll, and yaw of the aircraft and instrument, as well as multi-path effects. The latter arises when the direct path of the signal is blocked, thus increasing the travel time of the respective laser pulse and decreasing the resulting

elevation estimate. The effect of the aircraft inertial navigation system pitch cancels when averaging and smoothing the observations, while the roll induces a cross-track error. Krabill et al, (2002) considered repeat ATM flights in 1993/1998 and 1994/1999 and found the effects to produce SEC errors up to 1 cm/yr. Atmospheric errors are on the same order of magnitude, and thus vertical errors are typically less than 10 cm.

The validation data uncertainty is also associated with errors from the surface roughness in the area in which the trend is derived, particularly along the ice margin where significant changes may occur within the 200 m distance used for overlapping trajectories. Furthermore, a low number of estimation points reduce the accuracy of the generated trend.

## 2.2 Validation procedure

As the validation data (ATM/ALS) and the SEC-product have different spatial resolution (250 x 250 m vs. 5 x 5 km), the first step in the validation procedure is to average the validation data at the native posting of the SEC posting. This is done by assessing the median value of observations within a given grid cell. Then this median value is subtracted from the radar SEC estimate, and the mean, median and standard deviation (STD) hereof are computed. So are the minimum and maximum differences. Most often, the median is more informative of the product performance, as both data set are subject to outliers and the coarser resolution of radar-SEC product induces larger negative biases at outlet glaciers. The radar-SEC

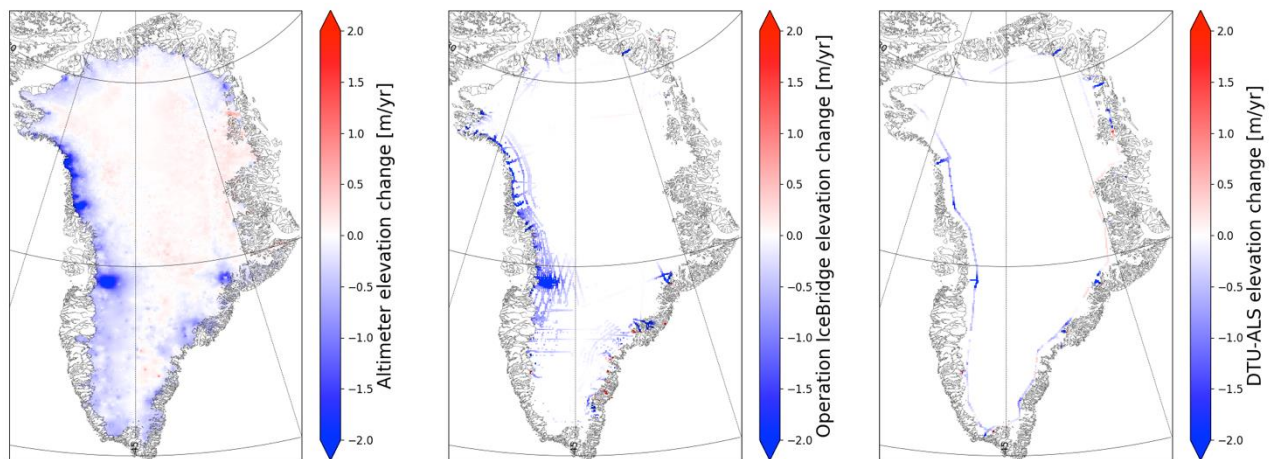


**Figure 2-1: : Data availability for the 2007-2011 SEC estimate (left). In the middle the elevation changes as recorded by the ATM-data set are shown and to the right the ALS elevation change data set.**

product consists of trends generated from combining all available ESA radar observation from 1992 to present and as five-year running means. The current 24 available SEC estimates are validated against the available validation data spanning the same time-windows. The region the ice sheet evaluated in each of the validation reports will differ from year to year due to differences in the flight paths from year to year of the airborne data. Figure 2-1 shows the spatial distribution of the available data from 2011 flights which approximately repeated the observations made in 2007.

### 2.3 Validation procedure outcome

The combination all available validation data (ATM/ALS) and the SEC-product produces a validation report for 19 of the 24 five-year running means in the SEC product, an example of the validation reports is shown in Figure 2-2. This report is typical for the time-slices but contains more data than the average example as both 2007 and 2011 had a lot of activity in Operation IceBridge and PROMICE. As observed with the different medians between the two validation data sets, the main bias between the airborne data and the SEC-product originates at the outlet glaciers. This may be attributed to slope-induced errors in radar data (Brenner et al. 1983; Roemer et al. 2007), which relocate the measurements up-slope from nadir and cause surface depressions such as the bottom of troughs and narrow valleys to be missed. The result is a very limited number of radar measurements inside the glacier trunks. Despite this, both the mean and STD are low relative to the min and max offsets, showing that radar data are indeed capable of resolving SEC even at the margin of the ice sheet.

	Operation IceBridge	DTU ALS	unit
number of data points	4411	1427	-
Mean difference	-0.28	-0.1	m pr. year
Median difference	-0.08	0.01	m pr. year
Standard deviation	0.88	0.67	m pr. year
Max. difference	6.84	5.55	m pr. year
Min. difference	-9.59	-7.82	m pr. year

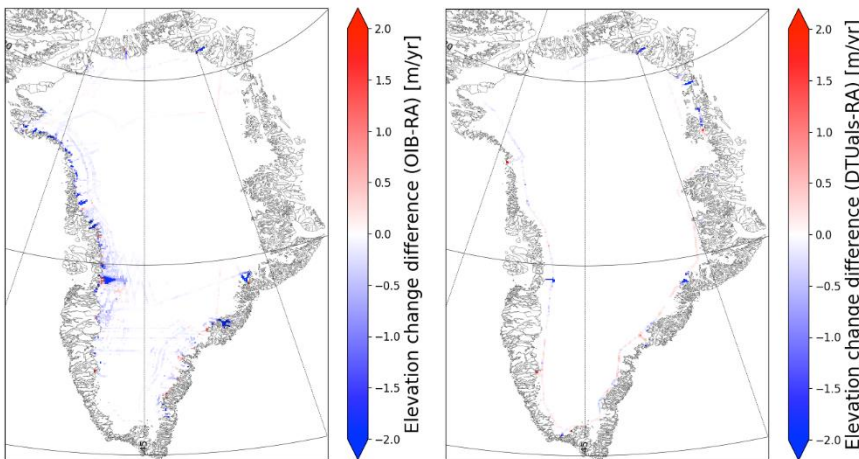


**Figure 2-2: Statics and spatial distribution of the 2007-2011 SEC estimate, as a result of the inter-comparison to the available airborne data.**

### 2.4 Recommendations for products improvement

One possibility for improving the SEC accuracy could be the use of a different retracker for the radar data. A number of studies have shown that such observations need to be adjusted for all three waveform parameters, i.e. the backscatter coefficient, leading edge width, and trailing edge slope, to ensure the highest accuracy (e.g. Khvorostovsky, 2012; Legresy et al, 2005, Simonsen and Sørensen 2017). However, as shown by Simonsen and Sørensen (2017) waveform corrections still leave a bias between the laser and radar estimated SEC, suggesting that a more surface-sensitive retracker could improve the laser-radar intercomparison. Another approach could be to implement waveform deconvolution to isolate surface elevation change (Slater et al 2019). Further research is needed to derive true surface elevation change from radar altimetry, but the implementation of the shaper waveform in SAR and SARIn seems a promising technological advance in retrieving this goal (McMillan et al. 2019). The novel swath processing of the Cryosat-2 should be implemented to enhance the resolution of the radar observations and gain more information about the spatial pattern of the elevation change happening in the high sloping areas. Work will be ongoing to estimate adaptability of the method. Another product improvement could be to increase the temporal resolution of the SEC. Although we are currently producing multi-year-trends because this suppresses the weather signal and isolates the climate signal, there might be users that would appreciate a higher temporal resolution.

## 3 Ice Velocity (IV)

### 3.2 Radar IV

The ice velocity (IV) product validation and intercomparison in this chapter provides an update of previous validation efforts, incorporating reprocessed velocity maps (version 1.3) and new and/or updated external validation datasets. The assessment is done for the annually-averaged ice-sheet wide velocity maps as well as the individual track maps (based on 6/12-day repeats) produced in the Greenland Ice Sheet CCI project and derived from Sentinel-1 (S1) SAR data. The individual track IV maps are the source data for the monthly and annually averaged maps. The quality assessment includes detailed validation with contemporaneous in-situ GPS data at various sites across the ice sheet. The products are also evaluated, on a pixel-by-pixel basis, against publicly available datasets covering the Greenland Ice Sheet. This product intercomparison provides a good level of quality assurance, in particular in areas where little change is to be expected. Additionally, we report on the performance of the algorithm in stable terrain, i.e. where no velocity is expected. This provides a good overall indication of the bias introduced in the end-to-end velocity processing chain including co-registration of images, velocity retrieval, etc. As no external validation data sets are available yet for the latest 2019/20 winter mapping campaign, this product is currently only included in the stable terrain analysis.

#### 3.2.1 Sources and selection of independent validation data

For in-situ validation, we use GPS data acquired by field teams of the Danish Programme for Monitoring of the Greenland Ice Sheet (PROMICE; Fausto and Van As, 2019) and available through the PROMICE Data Portal (<https://promice.org/PromiceDataPortal/>). The GPS instruments are attached to Automatic Weather Stations (AWS) operated by GEUS in collaboration with DTU Space and Asiaq. The version 3 data set provides hourly, daily and monthly average positions. Figure 3-1 shows the locations of the GPS sites used for validation.

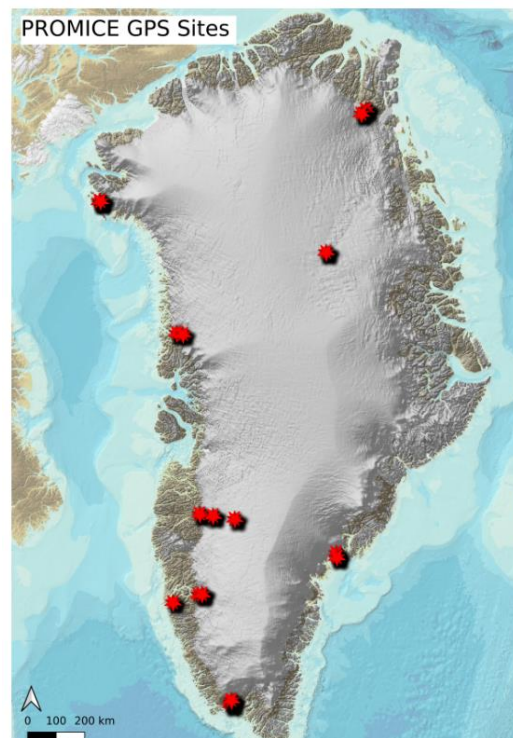


**Figure 3-1: Locations of the PROMICE AWS stations equipped with GPS and used for validation.**

For the product intercomparisons we utilize two different products created as part of the NASA 'Making Earth System Data Records for Use in Research Environments' (MEaSUREs) project: 1) annual Greenland wide IV map based on multi-mission SAR satellites; 2) IV maps covering main outlet glaciers and based on higher resolution TerraSAR-X (TSX) and TanDEM-X (TDX) data.

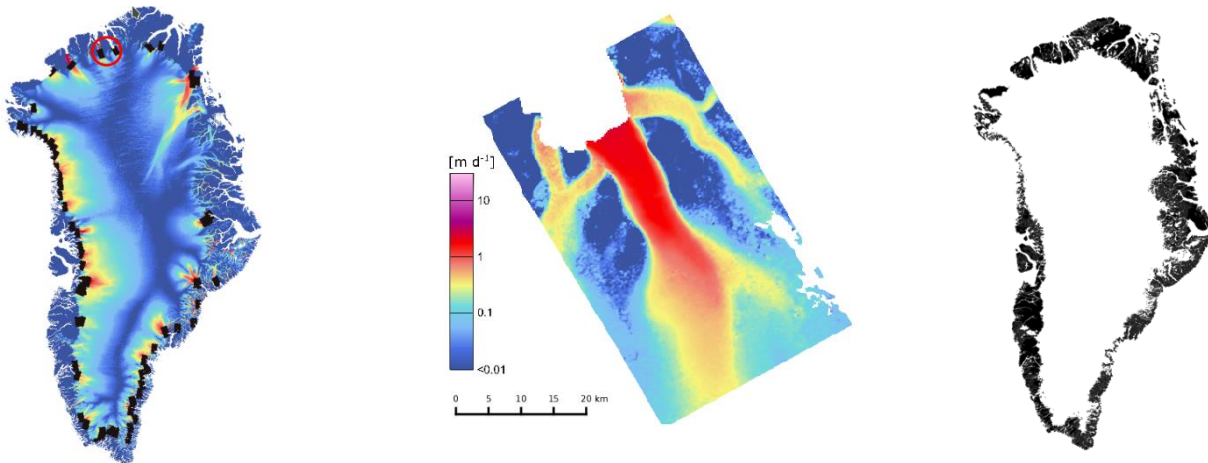


**Figure 3-2: Sentinel-1 IV mosaic showing locations of MEaSUREs TerraSAR-X/TanDEM-X derived IV maps used for product inter-comparison in black (left). The IV data sets cover the margins of Greenland and include most of the major outlet glaciers. The red circle indicates the location of C.H. Ostenfeld Glacier shown as example (middle). Right: shapefile showing ice-free terrain in Greenland and used for the stable terrain test (Rastner et al., 2012, updated 2018).**

The MEaSUREs annual Greenland-wide data set covers selected years since 2000 up to 2018 and is provided at 200 m and 500 m. The IV maps are based on multiple SAR satellites including: ALOS, RADARSAT-1, SENTINEL-1A and -1B, TDX and TSX. From 2014 onwards the maps are mostly based on Sentinel-1 data, supplemented with TSX and TDX data for coastal outlets. The annual maps run from September to May largely overlapping with the CCI products which run from October to September. We use version 2 of the data set, available through the NSIDC data portal (data set ID: NSIDC-0478, Joughin et al., 2015, updated 2018).

The MEaSUREs TSX/TDX-based data set consists of a collection of IV maps covering most of the major outlet glaciers from January 2009 to December 2019 (Figure 3-2, left and middle). The ice velocity is retrieved from repeat pass images (1 to 3 cycles with 11-day repeats) applying a combination of conventional InSAR and speckle tracking techniques (Joughin, 2002). Here we use release V3.0 of the data set, available through the NSIDC data portal (data set ID: NSIDC-0481, Joughin et al., 2020). Data files are delivered in GeoTIFF format at 100m grid spacing in North Polar Stereographic projection (EPSG: 3413). Separate files are provided for the x and y velocity components (in m/yr) along with corresponding (pseudo-)error estimates for both velocity components.

For the analysis of stable terrain, the moving ice is masked out using a polygon shapefile of the ice sheet and peripheral glacier outlines produced by Rastner et al (2012, updated 2018). The outlines are derived semi-automatically from Landsat-5 and Landsat-7, using a band ratio approach (red/SWIR) with scene specific thresholds and manual correction of debris cover, seasonal snow, shadow, water (outside of glaciers), sea ice and icebergs. By inverting the ice sheet/glacier shapefile and combining with an ocean mask a land mask file is created as depicted in Figure 3-2 (right).

### 3.2.2 Validation procedure

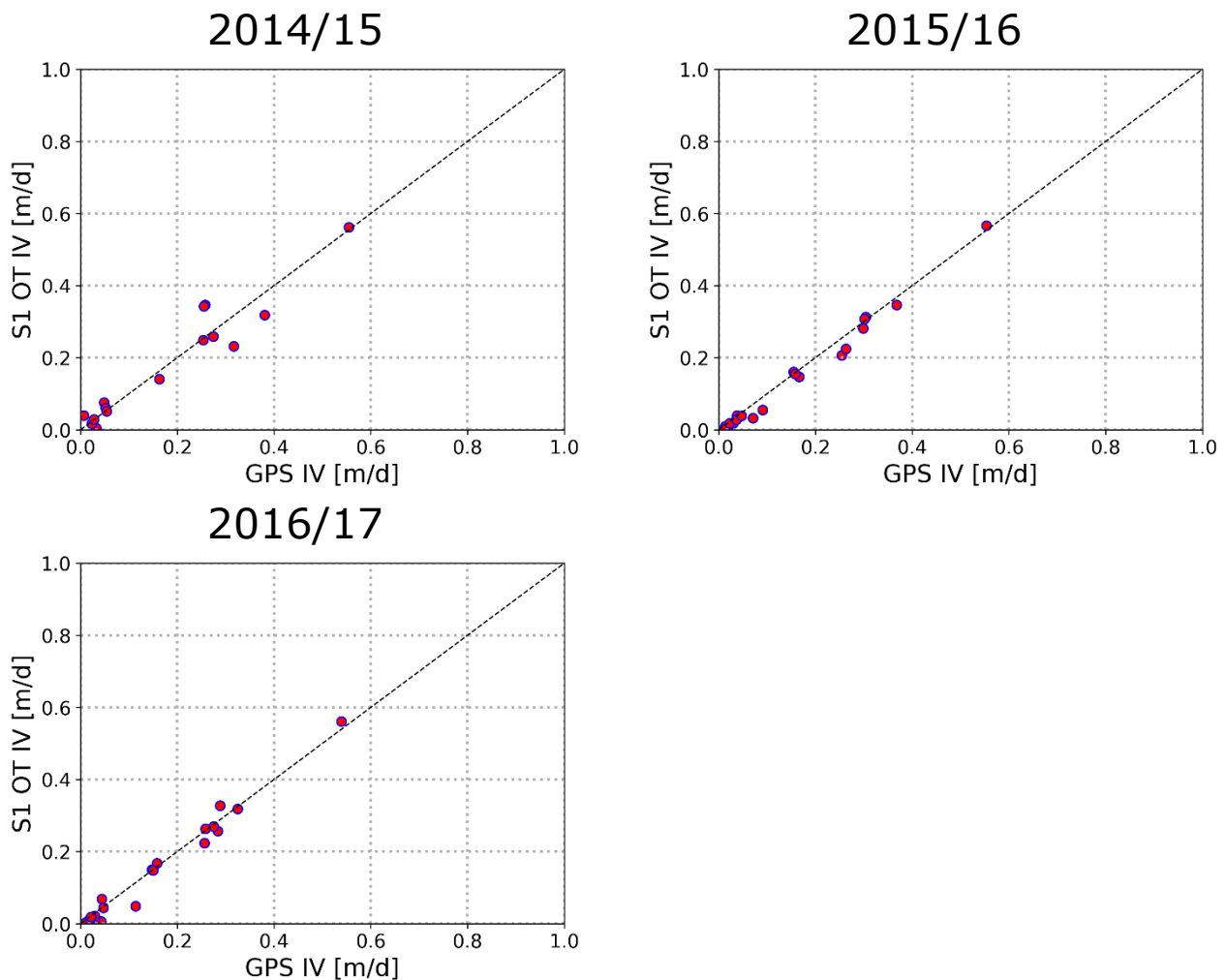
We use four different validation/intercomparison procedures, e.g. for GPS, product intercomparison and stable terrain analysis:

1. GPS: We use the monthly average positions provided in version 3 of the PROMICE AWS data set to calculate the local monthly averaged velocity magnitude, which is assigned to the station position. The monthly values are used to calculate yearly averages for Oct-Sept corresponding to the respective ice velocity map. For each monthly position, the corresponding pixel value in the Sentinel-1 IV map is selected and finally also averaged over a year. In this way there is one corresponding value for each station representing the annual mean IV. These are used to calculate the validation statistics and to create the scatter plots.
2. MEaSURES Greenland Ice Sheet Velocity Map: As a pre-processing step, the 200m IV maps are converted to m/d, resampled to a 250 m grid spacing and the separate Vx and Vy velocity files are merged into a 2-bands GeoTIFF to match the native Sentinel-1 IV maps geometry and format. The intercomparison is done on both the x and y velocity components separately on a pixel-by-pixel basis (ignoring the vertical component of velocity).
3. MEaSURES TSX/TDX-based IV maps: Pre-processing is similar as described above. As glacier velocity can fluctuate significantly over short time periods, in particular on the downstream section of large outlet glaciers, we only compare datasets derived from single Sentinel-1 SAR repeat pass pairs (6/12-days) and with a maximum time difference of 2 days between the respective start dates (master). We inter compare both x and y velocity components separately on a pixel-by-pixel basis.
4. Stable terrain analysis: The results for the ice covered (moving) area are separated from ice-free (stable) ground. The masking is done using a polygon of the rock outlines.

As a measure of quality, we provide, statistics on the mean and the root mean square error (RMSE) of the residuals (defined here as Sentinel-1 IV minus GPS/MEaSURES IV).

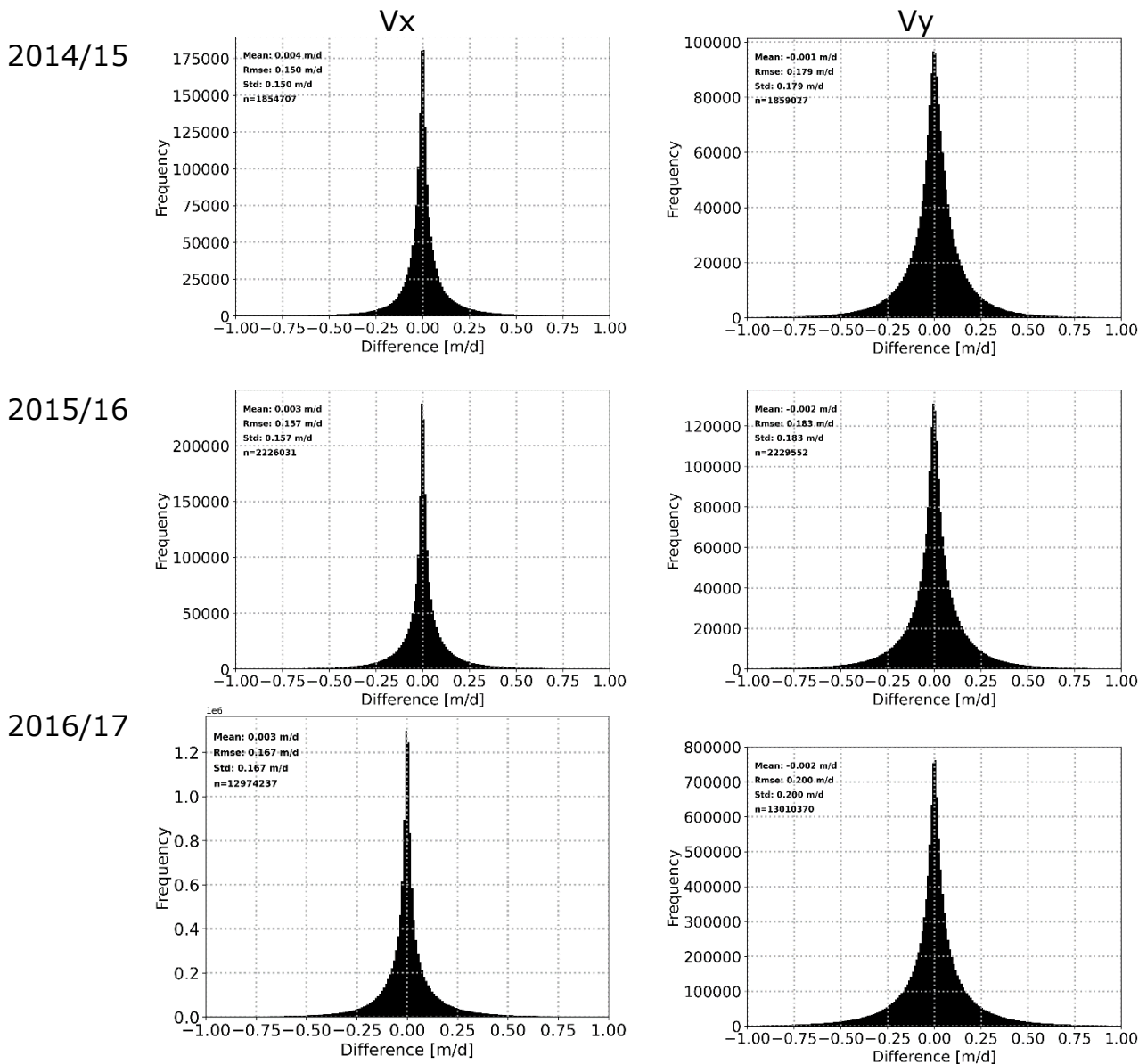
### 3.2.3 Validation procedure outcome

Figure 3-3 shows the results of the intercomparison of the annual Sentinel-1 Greenland Ice Sheet velocity with in-situ GPS measurements for 2014/15, 2015/16 and 2016/17 (v1.3). The figures show an excellent agreement between the GPS and Sentinel-1 surface velocity. For 2014/15 a total number of 15 stations could be used, with a mean difference <1 cm/d and an RMSE of 4.5 cm/d. In 2015/16 22 stations could be used showing a mean difference of 1.2 cm/d and an RMSE of 2 cm/d. In 2016/17 also 22 stations could be used with a mean difference of 1.1 cm/d and an RMSE of 3 cm/d. The observed differences can partly be attributed to uncertainties inherent to both methods including differences in spatial sampling: the GPS measures a point location, while the feature tracking procedure averages an area of which the size is based on the window size used for image correlation.



**Figure 3-3: Scatter plots of GPS and Sentinel-1 ice velocity for 2014/15, 2015/16 and 2016/17.**

Excluding the TSX/TDX derived IV maps that do not fall within the desired temporal range (max time difference 2 days in comparison to S1 IV maps) leaves a total number of 123, 230 and 376 suitable TSX/TDX IV maps for product intercomparison for respectively 2014/15, 2015/16 and 2016/17. For each TSX/TDX derived IV map multiple intercomparisons are possible as an area can be overlapped by different S1 tracks over the 2-day time range. In total 168 (2014/15), 312 (2015/16) and 1231 (2016/17) Sentinel-1 maps fulfil the 2-day criterium and also have an overlap. For these maps, the residuals and their statistics are calculated (Figure 3-4). The overall mean bias between the data sets is well below 1 cm/d with an RMSE in the range of 15-20 cm/d for both x and y velocity components.



**Figure 3-4: Histograms of Vx (left) and Vy (right) residuals of the intercomparison with MEaSURES TerraSAR-X derived IV maps (selected outlet glaciers) acquired within 2 days of Sentinel-1 derived single track IV maps in 2014/15 (top), 2015/16 (middle), 2016/17 (bottom).**

Figure 3-5 shows the intercomparison results of the GIS CCI annual ice sheet wide IV maps of 2014/15, 2015/16 and 2016/17 with the MEaSURES IV maps for the same years. Based on a sample size of >30 million pixels for each map comparison, the overall mean bias between the two data sets is less than 2 mm/d with an RMSE in the range of 3 to 6 cm/d for both x and y velocity components.

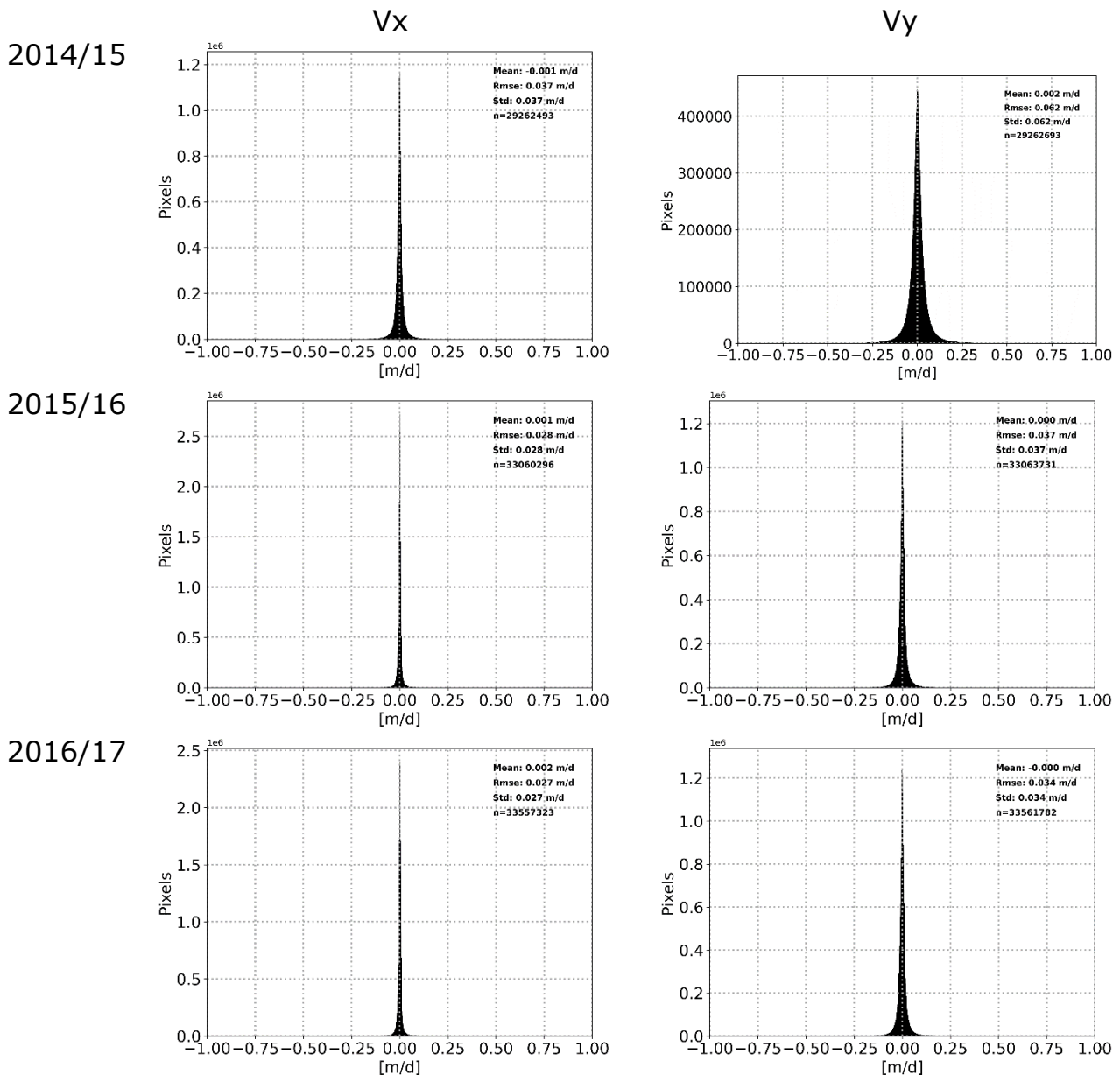


**Figure 3-5: Histograms of Vx (left) and Vy (right) residuals of the intercomparison between the CCI Greenland Ice Sheet velocity maps (v1.3) and MEAsURES in 2014/15 (top), 2015/16 (middle), 2016/17 (bottom).**

Differences between the products have a variety of causes, among others the different native resolution of the SAR data (e.g. TSX vs. Sentinel-1), different temporal range, different processing settings used for IV retrieval (e.g. matching window, correlation threshold), differences in post processing (e.g. outlier removal, gap filling), different land/ocean and lay-over masks or short term velocity fluctuations. In general, higher resolution satellite data better captures the ice velocity, in particular in shear zones, where the velocity gradient can be high. The drawback often being that much smaller regions are covered.

Figure 3-6 shows the results of the stable terrain test as scatterplots of easting versus northing velocity for all maps, including the 2019/20 winter mapping campaign (CCI v1.3). Based on more than 1.2 million pixels the outcome of the stable ground test indicates for all products a mean of <1 cm/d and an RMSE < 2 cm/d for both easting and northing velocity components.

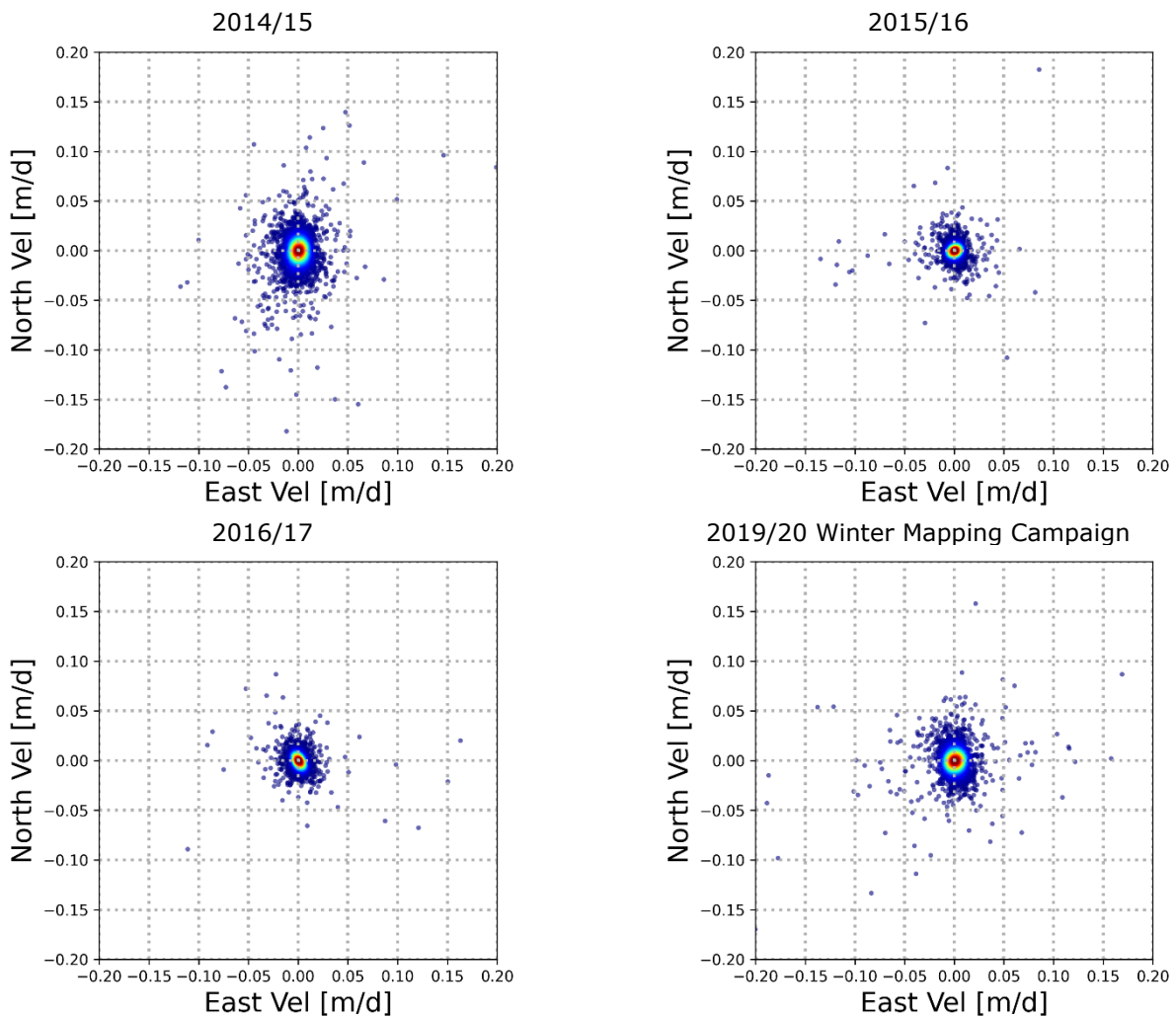


**Figure 3-6: Results of the stable rock test for the different CCI+ velocity products. The scatter plots show easting velocity versus northing velocity with colour coding blue to red indicating point density from low to high.**

### 3.2.4 Recommendations for products improvement

Table 3.3 provides a statistical overview of all validation and intercomparison results. The current IV products perform very well. The accuracy requirements for IV as described in the User Requirements Document (URD) of the Ice Sheets CCI project (Hvidberg, et al, 2012), identified through an extensive user survey within the glaciology community, lists a minimum accuracy of 30-100 m/y (0.08-0.27 m/d) with an optimum accuracy of 10-30 m/y (0.03-0.08 m/d). The results of our quality assessments fall well within this range. A key product improvement for IV is the InSAR processing which currently under development within the CCI+ project and which is expected to be included in cycle 2 of the document. The development is expected to significantly improve the accuracy of the ice velocity, in particular in slower moving terrain.



**Table 3.3: Summary of intercomparison results (values in m/d).**

Product	Reference/Test	Pixels	d <sub>Mag</sub>	RMSE <sub>Mag</sub>	d <sub>E</sub>	RMSE <sub>E</sub>	d <sub>N</sub>	RMSE <sub>N</sub>
2014/15	GPS	15	0.00	0.05	-	-	-	-
	MEaSURES TSX/TDX	1.8 M	-	-	0.00	0.15	0.00	0.18
	MEaSURES S1 (ice sheet)	29 M	-	-	0.00	0.04	0.00	0.06
	Stable Terrain	5 M	-	-	0.00	0.01	0.00	0.02
2015/16	GPS	22	0.01	0.02	-	-	-	-
	MEaSURES TSX /TDX	2.2 M	-	-	0.00	0.16	0.00	0.18
	MEaSURES S1 (ice sheet)	33 M	-	-	0.00	0.03	0.00	0.04
	Stable Terrain	5 M	-	-	0.00	0.01	0.00	0.01
2016/17	GPS	22	0.01	0.03	-	-	-	-
	MEaSURES TSX/TDX	13 M	-	-	0.00	0.17	0.00	0.20
	MEaSURES S1 (ice sheet)	34 M	-	-	0.00	0.03	0.00	0.03
	Stable Terrain	5 M	-	-	0.00	0.01	0.00	0.01
2019/20 winter mapping campaign	Stable Terrain	5 M	-	-	0.00	0.02	0.00	0.01

### 3.2.5 Acknowledgments of data contributors for IV validation

Data from the Programme for Monitoring of the Greenland Ice Sheet (PROMICE) and the Greenland Analogue Project (GAP) were provided by the Geological Survey of Denmark and Greenland (GEUS) at <http://www.promice.dk>. Data from the NASA Making Earth System Data Records for Use in Research Environments (MEaSURES) Program were provided by the National Snow and Ice Data Center (NSIDC) at <https://nsidc.org/data/measures>.

### 3.3 Optical IV

#### 3.3.1 Sources and selection of independent validation data

In order to validate the Sentinel-2 based optical IV products both in situ data and IV derived from other EO sources were considered. The main source of in situ data is the GPS data gathered by the Promice weather stations, however these stations are located on the ice sheet or relatively slow-moving ice rather than on the fast-flowing outlet glaciers. Since the optical IV products are focussed on the fast-flowing outlet glaciers, relevant in situ data is not available to our knowledge. The main alternative EO data source to derive IV from are SAR measurements. Both Promice and Enveo have produced SAR based products from Sentinel-1 with good spatial temporal coverage allowing for a comparison with the Sentinel-2 optical based IV. Therefore, the two main sources that were selected for an independent validation are:

- 1) Promice Sentinel-1 (SAR) based IV
- 2) Enveo Sentinel-1 (SAR) based IV

#### 3.3.2 Validation procedure

For the validation it was decided to compare monthly products, because these products could be derived for all three IV datasets. In the case of Enveo monthly products can be downloaded directly. The Promice IV data products have a time span of 23 days with 50% temporal overlap to the next product. By merging two products roughly monthly products can be derived. For the optical IV a timespan of a month often is long enough to have sufficient cloud free imagery to derive an IV product. Based on the available data for all sources 3 monthly products for different outlet glaciers during the 2019 summer season were selected:

- 1) Jakboshavn august 2019
- 2) Petermann july 2019
- 3) Upernavik july 2019

The three different IV datasets (S&T, Enveo and Promice) come at different resolutions and grids. To allow for a direct comparison the S&T and Promice datasets are re-gridded to 250m resolution to match the resolution and grid of the Enveo dataset. The IV magnitude of the reference products is subtracted from optical IV to derive IV offset maps.

#### 3.3.3 Validation procedure Outcome

The overall trend in IV is similar to the one observed in the SAR based products of both Enveo and Promice (see figure Figure 3-7). In regions of low ice flow velocity, typically speeds are higher in the optical product. This is likely due to the limitations within the co-registration process. Furthermore, it should be noted that post processing steps, such as interpolation, smoothing and filtering, likely vary for the different datasets

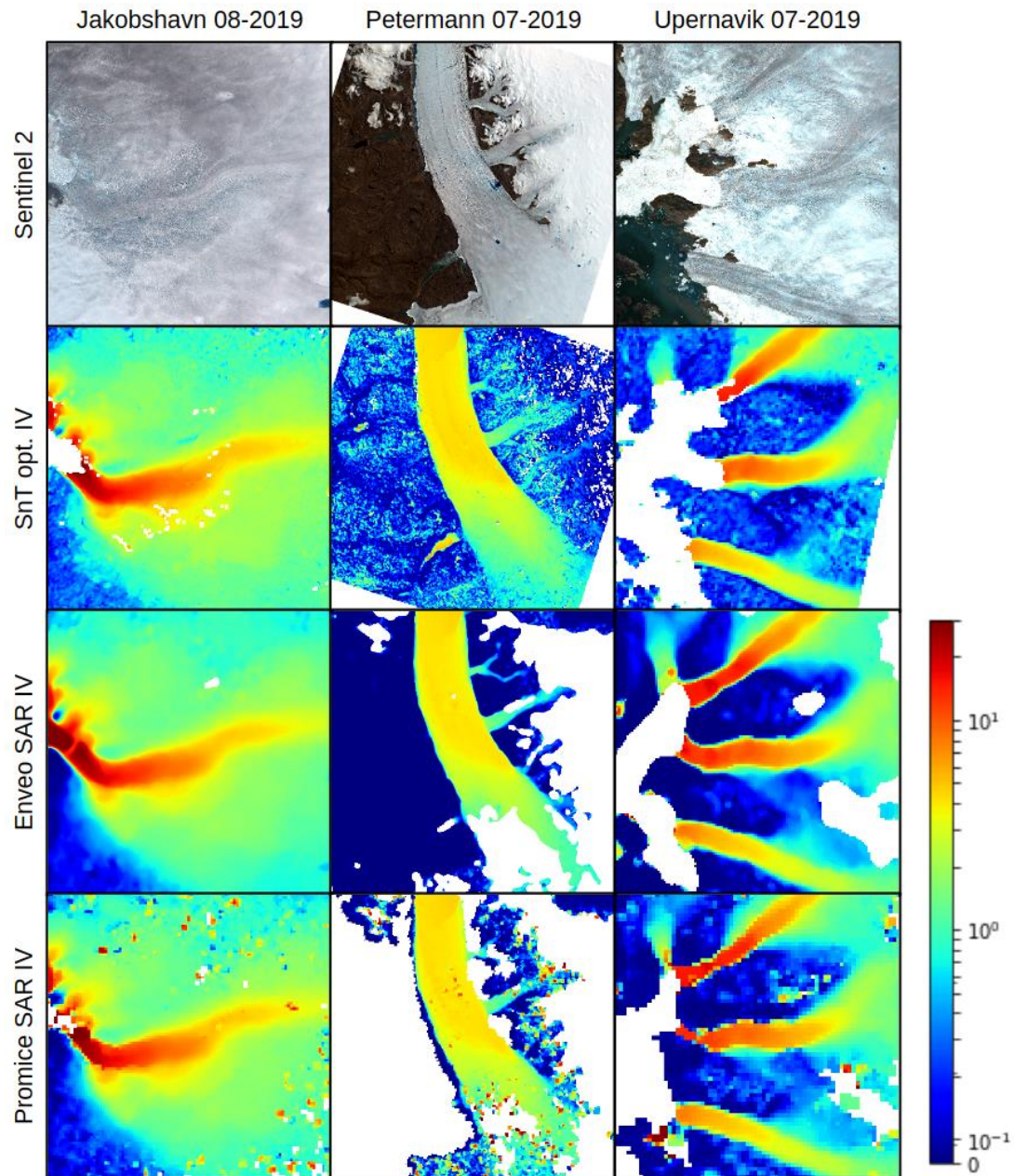


**Figure 3-7: Comparison of S&T, Enveo and Promice IV datasets for three different outlet glaciers. Speed is given in [m/day].**

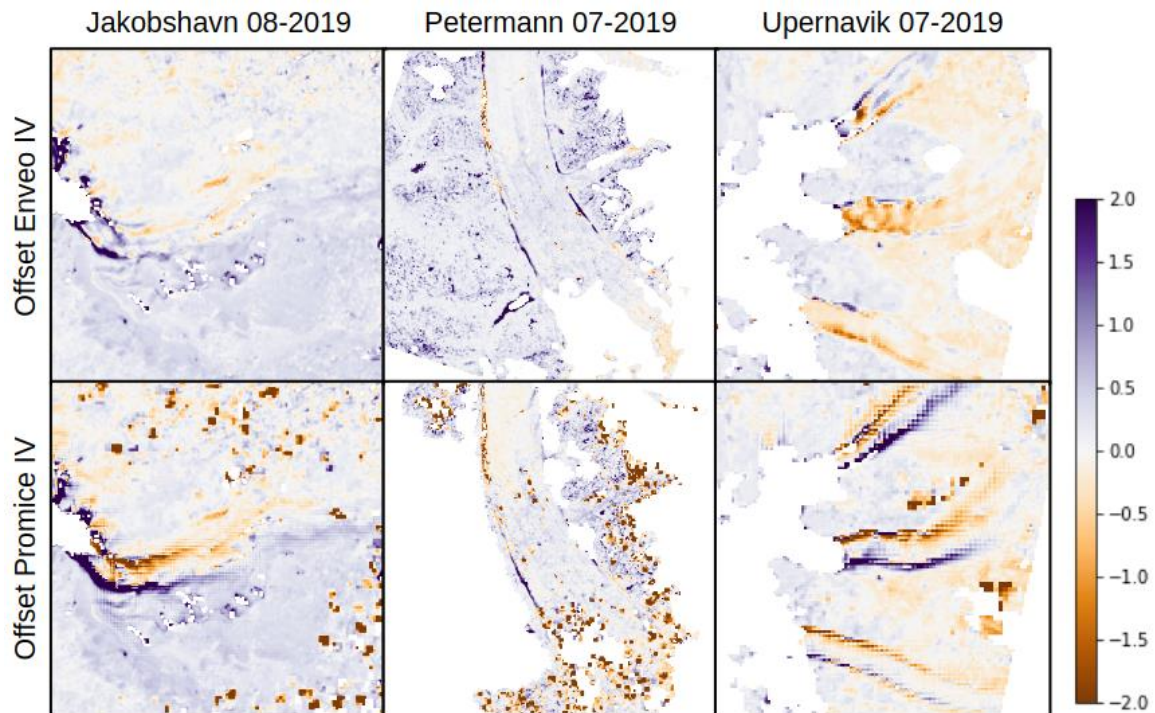


**Figure 3-8: IV offsets of S&T optical IV compared to Enveo and Promice SAR IV. Offsets are given in [m/day].**

Figure 3-8 shows the IV offsets between the S&T optical products compared to the Enveo and Promice SAR products. Speeds are generally the same order of magnitude, with maximum offsets at around 2m/day. Large offsets can be due to artefacts in the data, this is especially the case for the Promice dataset. In addition, large offsets can be observed along the margins of the fast-flowing ice, this is at least partly due to interpolation errors, keeping in mind that the initial resolution of the Promice dataset is 500m. In the offset images it can also be seen that optical based IV is slightly higher in areas of slow-moving ice, this is likely due to the co-registration issue described above. For the fast-flowing ice in Petermann IV is higher whilst for Upernavik speeds of the fast-flowing ice are slightly lower. These offsets could be due to many limitations within the optical and SAR methods. For the optical main error sources are imperfect pixel matching, co-registration, and a lack of a complete time series due to cloud cover. Furthermore, the IV maps are generated from a time series of imagery and Sentinel-2 and Sentinel-1 don't match perfectly in time. The histograms in Figure 3-9 show the difference for the offsets in the low IV (< 0.4) and high IV (> 4) more clearly.

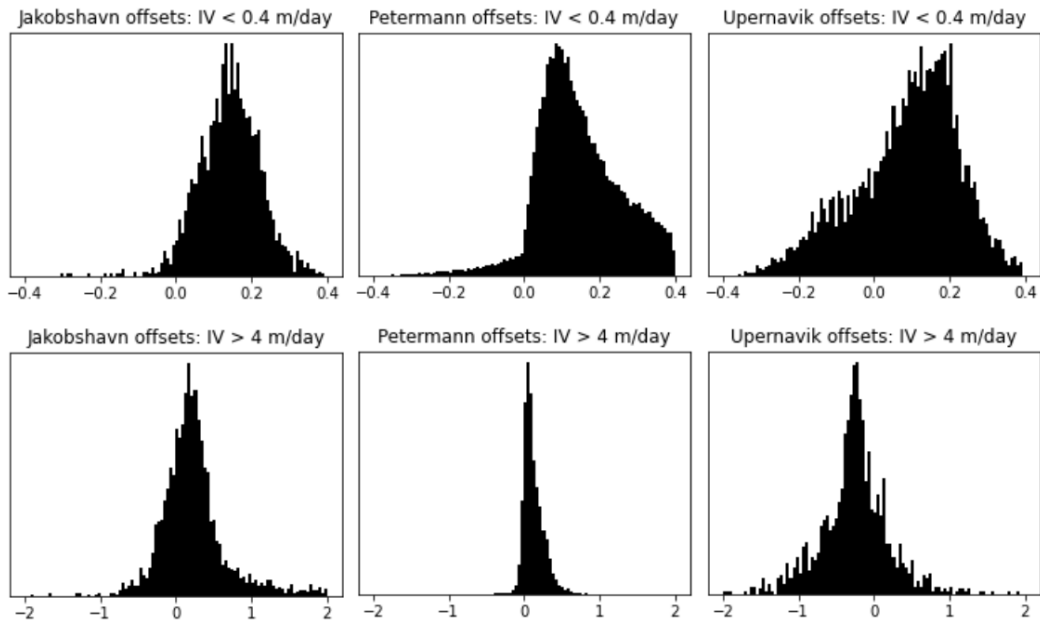


**Figure 3-9: IV offsets of S&T optical IV compared to Enveo SAR IV. Offsets are given in [m/day].**

### 3.3.4 Recommendations for products improvement

The basis of the optical IV algorithm is the matching of pixels to determine a shift. Together with the time difference between two images this allows to derive IV. Improvements to the feature tracking algorithm which does the matching will therefore directly impact results. Possible improvements are exploiting multiple bands and increasing storage of pixel from 8 to 16 bit. Both are ways to exploit more information that is present in the Sentinel-2 imagery. Additionally, co-registration could maybe be improved, currently only a single x/y shift is found and used for correction. However, more complex warping effects are present in the data especially in areas with a lot of topography. Finally, some manual work is still required to run the whole processing chain, such as checking the selection of cloud free scenes. Improvements to cloud masking could automate this step.

## 4 Gravimetry Mass Balance (GMB)

This chapter gives a summary of the activities carried out to assess the quality of the GMB products.

There has been no direct validation of the GMB products because no independent data sets are available. Instead inter-comparisons have been carried out to assess the variability of these products arising from the use of different methods and data sets.

Previously, several inter-comparison exercises have been carried out. The results of these together with further investigations made on the specific CCI products are presented here.

### 4.1 (Inter-) comparison procedure

There are several (inter-)comparison strategies to follow. We focus on the mass change time series (and the trend in this) product and describe the following:

1. Comparison to other methods for regional and ice sheet mass balance. These are the Input-output method (or mass budget method) and volume change method.
2. Inter-comparison of the results from different methods for deriving mass changes from the same GRACE data
3. Inter-comparison of the results from using the same method but different data sets.

### 4.2 (Inter-) comparison procedure outcome

1. A comparison of GRACE-derived mass changes to other methods for regional and ice sheet mass balance is a major task to undertake, and outside the scope of this document. Several of such studies have been published, and here we highlight a few. The IMBIE (international mass balance inter-comparison experiment, Shepherd et al., 2012, 2018 and 2020) was an ambitious project including numerous methods and data sets.

The overall mass balance for ice sheets from different methods is seen in Fig 4-1. These are the Input-output method (or mass budget method) and volume change method.

It can be seen that the gravimetry method predicts mass balance results that agree with the two other methods within the error bars. Both methods, i.e. the point mass inversion and the tailored sensitivity kernel approach, which are used for generating the GIS CCI GMB products (see AD5) were also provided to the IMBIE study (Shepherd et al., 2018 and 2020).

2. A detailed inter-comparison of the results from different methods for deriving mass changes applied on the same GRACE data was undertaken in the CCI GMB Round Robin Exercise (RRE). The procedure and the results are described in detail in Groh et al. (2019). Both methods used in the GIS CCI GMB production were included in the RRE and showed good agreement with other submissions.

The RRE participants were anonymized, but Fig. 4-2 shows the good agreement between the GIS CCI GMB products derived by DTU and TUDr (for the entire GIS). Figure 4-3 and 4-4 also shows the other drainage basin mass change time series. The two products show very small differences only in few basins and all the differences are within the error bars.

3. The third strategy is the inter-comparison of results from using the same method but different data sets. Figure 4-5 shows the mass change time series based on two data sets: CSR05 and ITSG2016. From this comparison no significant differences are seen between the two data sets.

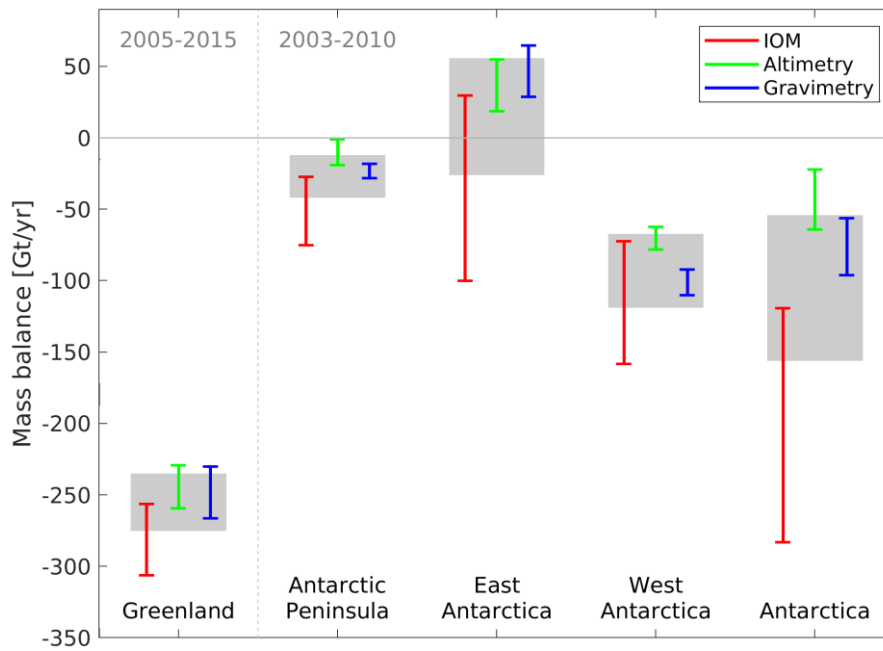


Figure 4-1: Mass balance of the ice sheets from different methods (Shepherd et al., 2018,2020).

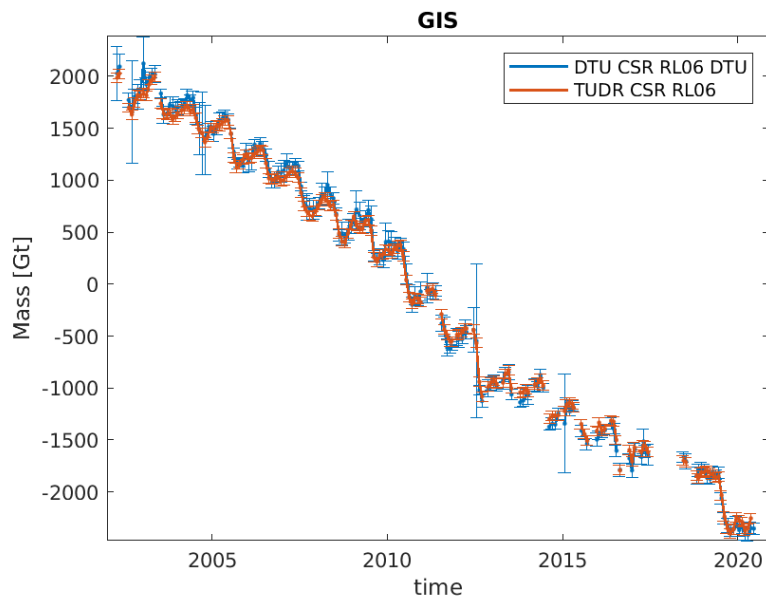
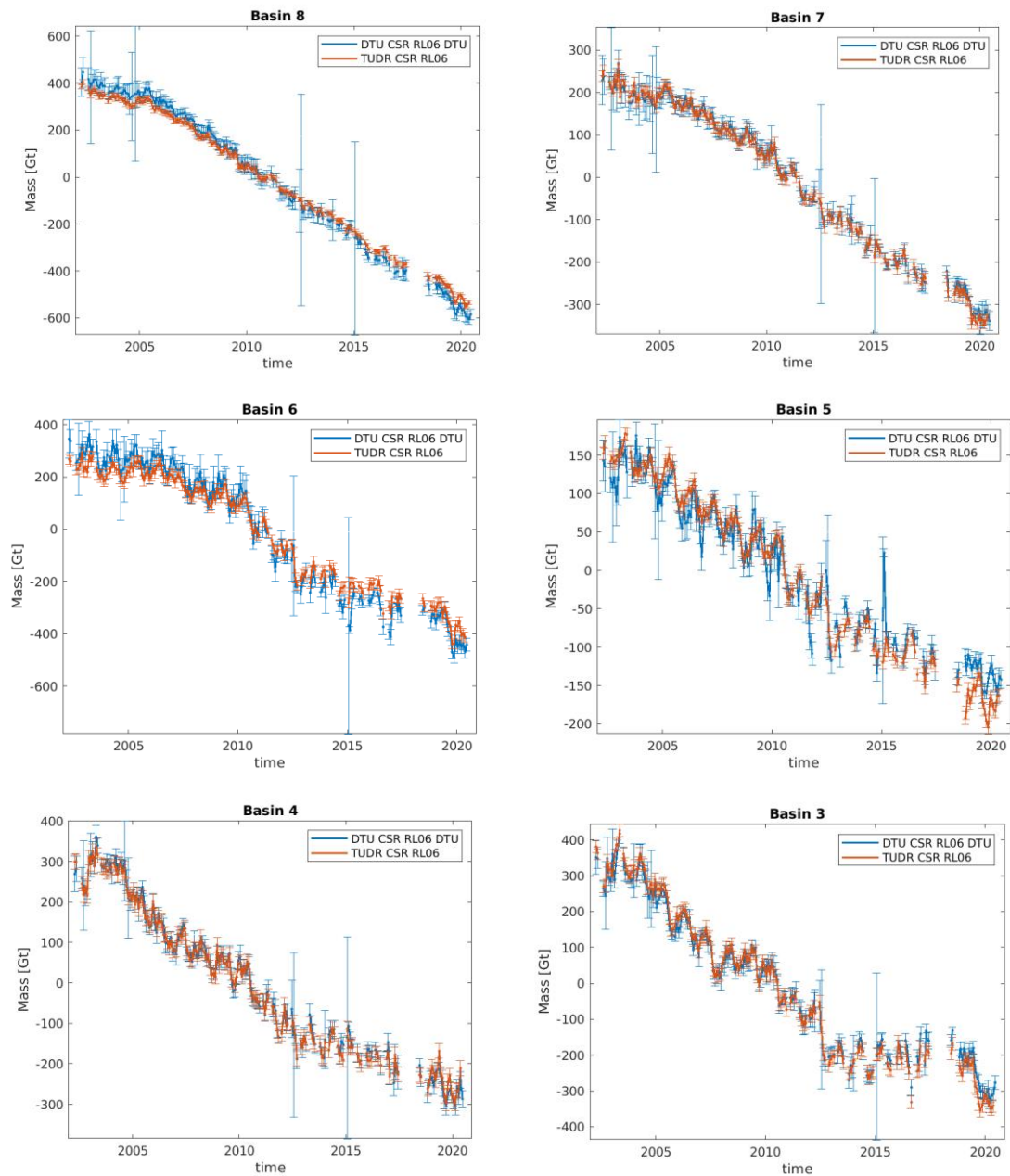
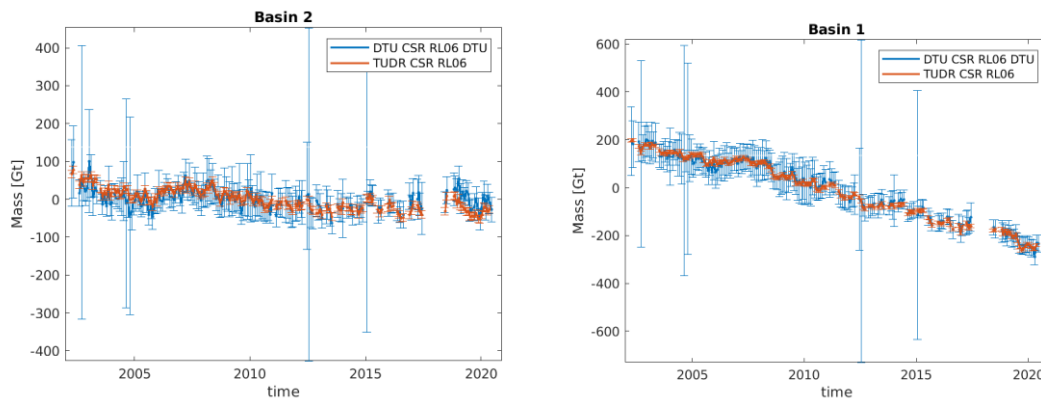


Figure 4-2: Mass change time series of the entire GIS, from the GIS CCI GMB products derived by DTU (blue) and TUDr (red).



**Figure 4-3: Mass change time series of basin 8 to 3 from the GIS CCI GMB products derived by DTU (blue) and TUDr (red).**



**Figure 4-4: Mass change time series of basin 1 and 2 from the GIS CCI GMB products derived by DTU (blue) and TUDr (red).**

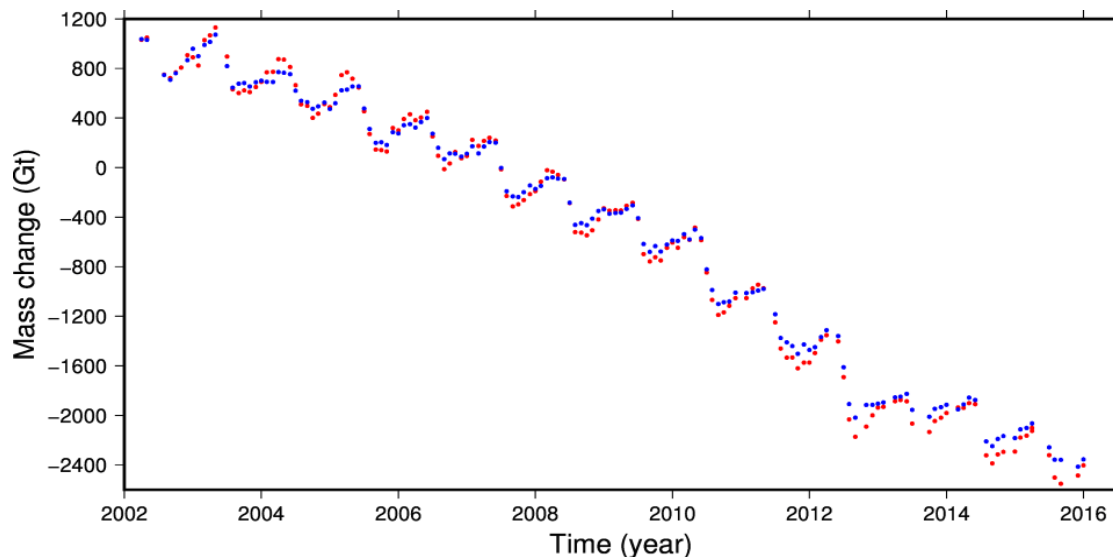


**Figure 4-5: Mass change time series derived from CSR05 data (red) and ITSG2016 (blue)**

### 4.3 Recommendations for products improvement

Better models for GIA, degree one, and ocean model correction will lead to future improvement in the products. Studies targeted on these corrections could lead to improvements in the products.

#### Integrated CryoSat, GRACE and Sentinel-1 data.

One issue with the GRACE-only products is the low spatial resolution and therefore one recommendation is to produce products with increased resolution. This could be done from integrated CryoSat, GRACE and Sentinel-1 data, combined with firn compaction and snow surface density meteorological models.

The mass changes of the Greenland ice sheet are measured directly with GRACE, but only with limited spatial resolution, and relatively large errors associated with leakage from oceans, land, and other ice caps. Combining CryoSat and GRACE data, supplemented with a firn density and compaction model, an integrated mass solution can be obtained with high spatial resolution. Noting that rapid temporal changes of the ice sheet is primarily driven by rapid changes in velocities of outlet glaciers, which can now be monitored at weekly resolution by Sentinel-1, the combination of all three EO data sources – GRACE, CryoSat altimetry and Sentinel-1 ice velocities – into a unified mass product, will give a new enhanced



experimental ECV product, superior to the existing CCI SEC, IV and GMB products. This enhanced product will represent an operational product following the IMBIE principles and can easily be extended to Antarctica as well at a later stage. The first concept demonstration results of such activities, for both Greenland and Antarctica, has been published in Forsberg et al. 2017.

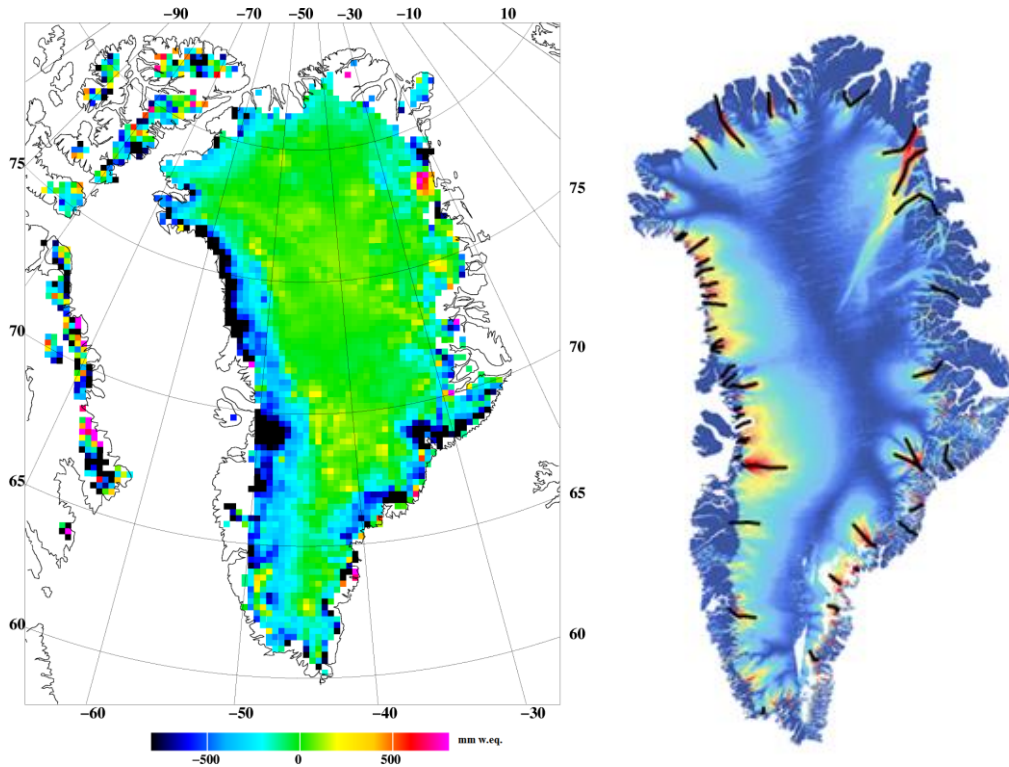


**Fig. 4-6. GRACE/CryoSat mass balance grid of Greenland (left, low-resolution demonstration product) will be combined with Sentinel 1-A (and later -B) ice velocities from the Greenland ice sheet (right) in the proposed CCN/CCI+ action. Current S-1 acquisition scheme allow sub-monthly estimation of essentially all Greenland outlet glaciers.**

## 5 Mass Flow Rate and Ice Discharge (MFID)

The MFID product is validated against all known estimates of ice discharge that are available at the spatial (sector, Zwally *et al.* (2012)) and at least annual resolution. This includes two completely independent plus one different dataset of ice discharge. The independent estimates come from external parties while the "different" dataset is produced by Ken Mankoff (producer of these CCI+ data), using a similar algorithm, but tuned differently. That is, the Mankoff *et al.* (2020) validation data set is generated with gates in different locations and using a different cutoff velocity than this CCI+ work.

### 5.1 Sources and selection of independent validation data

Independent data comes from King *et al.* (2020), Mouginit *et al.* (2019), and Mankoff *et al.* (2020). King *et al.* (2020) provides discharge estimates at monthly temporal and glacier spatial resolution. Mouginit *et al.* (2019) provides discharge estimates at *annual* temporal and sector spatial resolution. Mankoff *et al.* (2020) provides discharge at ~12-day temporal and glacier spatial resolution. Although Mouginit *et al.* (2019) is only annual resolution, this should not significantly impact results which according to King *et al.* (2018) only vary by ~6 % seasonally.

### 5.2 Validation procedure

We downsample the Mankoff *et al.* (2020) and King *et al.* (2020) data to monthly temporal and basin spatial resolution, by averaging in time and summing in space, and then compare to this product that already exists at that resolution. The Mouginit *et al.* (2019) product remains at annual temporal resolution. We then graphically display this product (CCI+), with all of the other products, in individual plots per sector (Zwally *et al.* (2012)). We then visually compare the lines in the graphics.

### 5.3 Validation procedure outcome

The lines all overlap within the uncertainty estimates. Some sectors do have outliers, but the CCI+ product is never the outlier. Therefore, the CCI+ product always falls within the uncertainty estimates of the majority of the other comparable discharge products.

### 5.4 Recommendations for products improvement

No recommendations at this time.

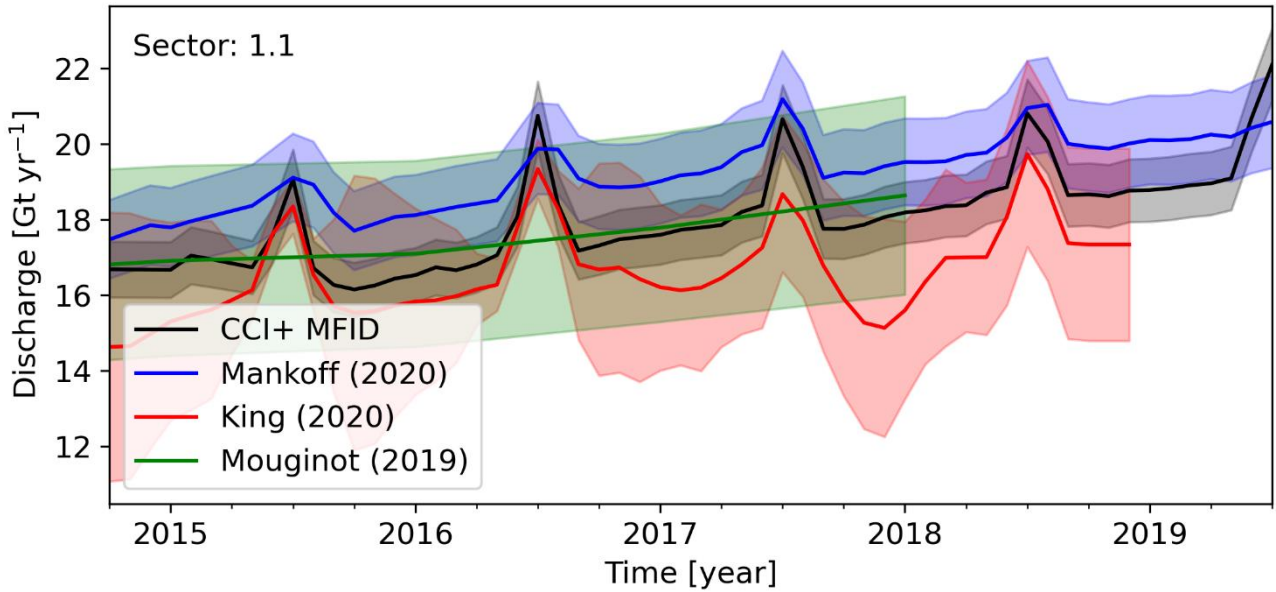


**Figure 5-1:** Comparison between this product (CCI+ MFD; black), Mankoff et al. (2020) (blue), King et al. (2020) (red), and Mouginit et al. (2019) (green). Uncertainty estimates come from the respective published products or described in the ATBD and uncertainty documentation for the CCI+ product. Sector label from Zwally et al. (2012) is printed in top-left corner of graphic.

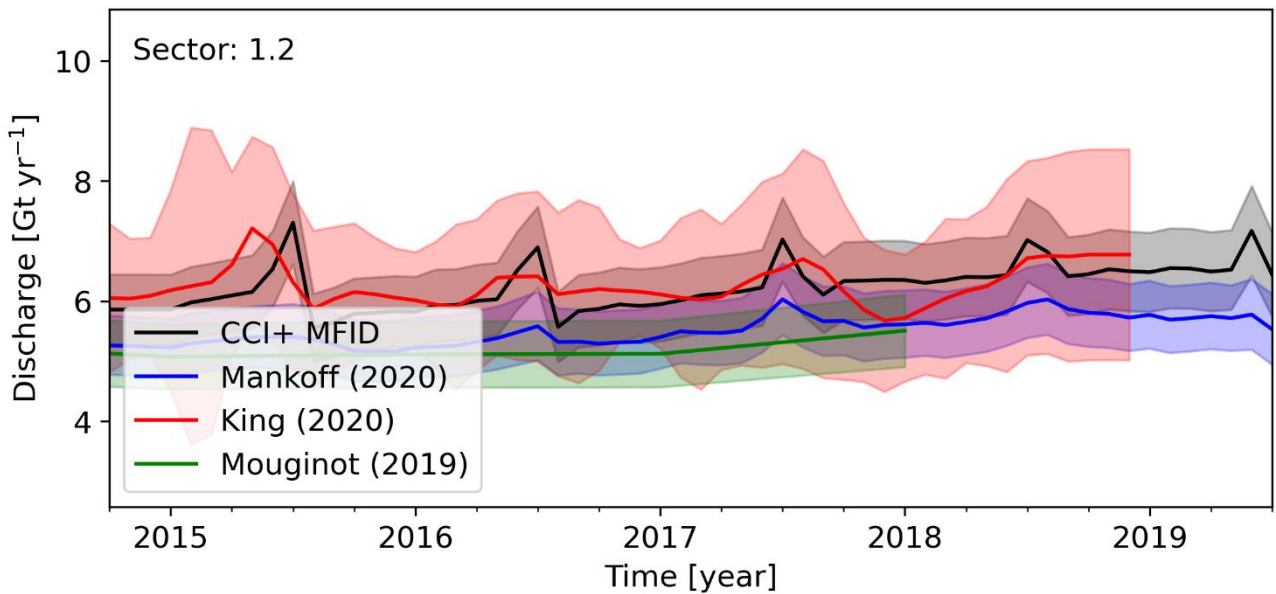


**Figure 5-2:** Same as Figure 5-1 caption.

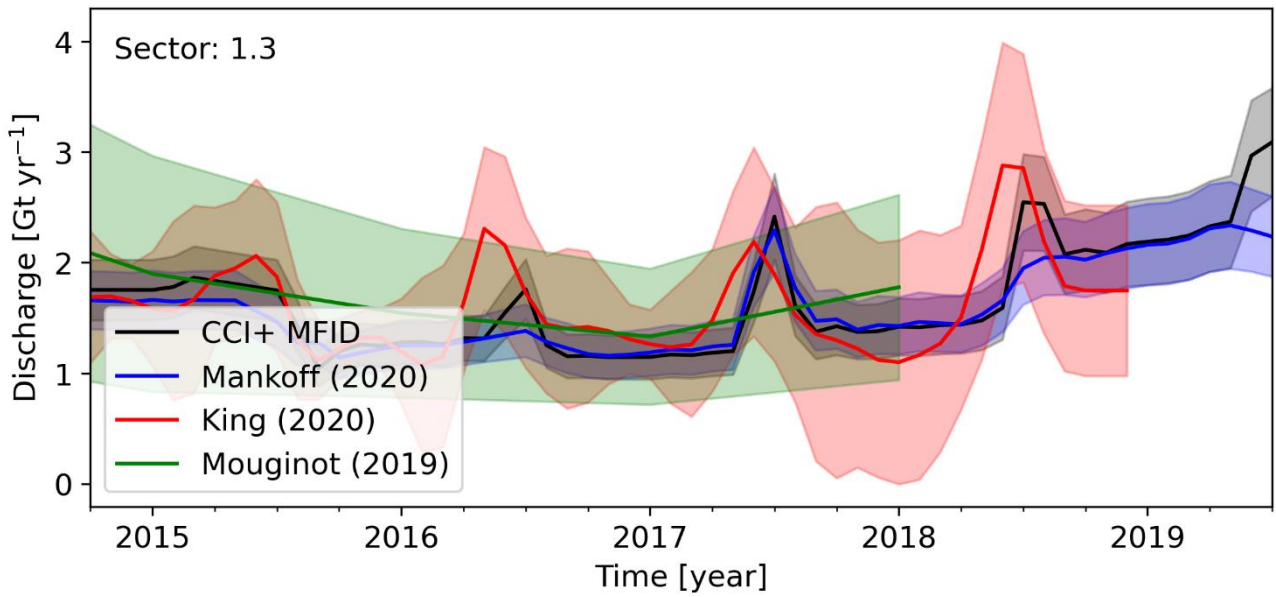


Figure 5-3: Same as Figure 5-1 caption.

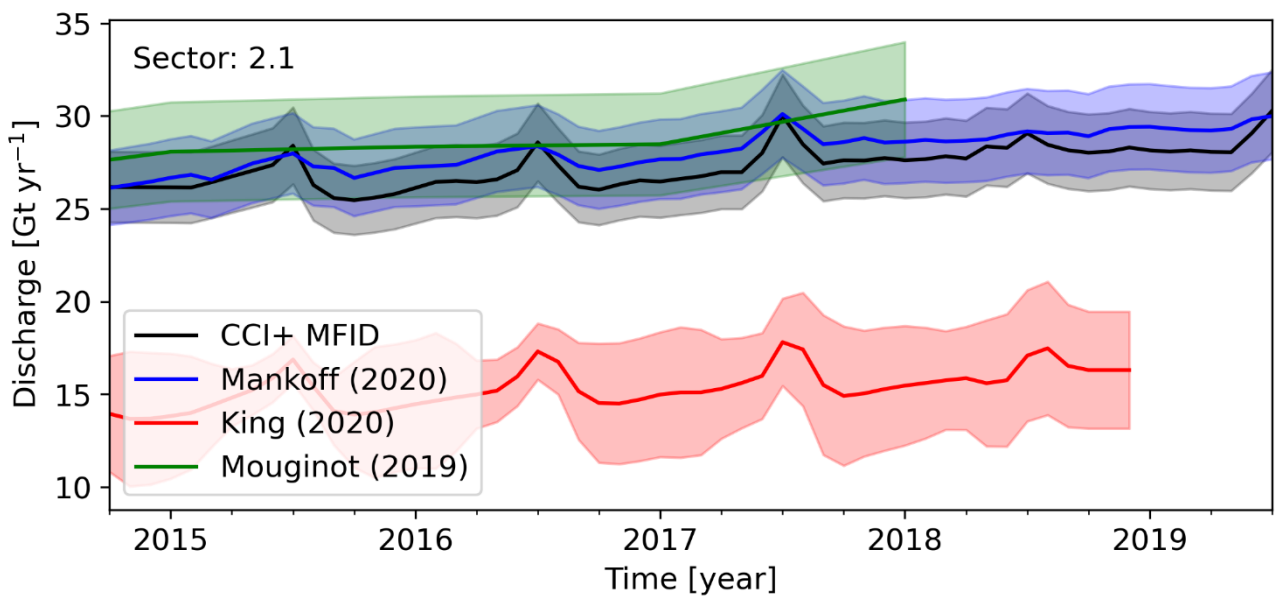


Figure 5-4: Same as Figure 5-1 caption.

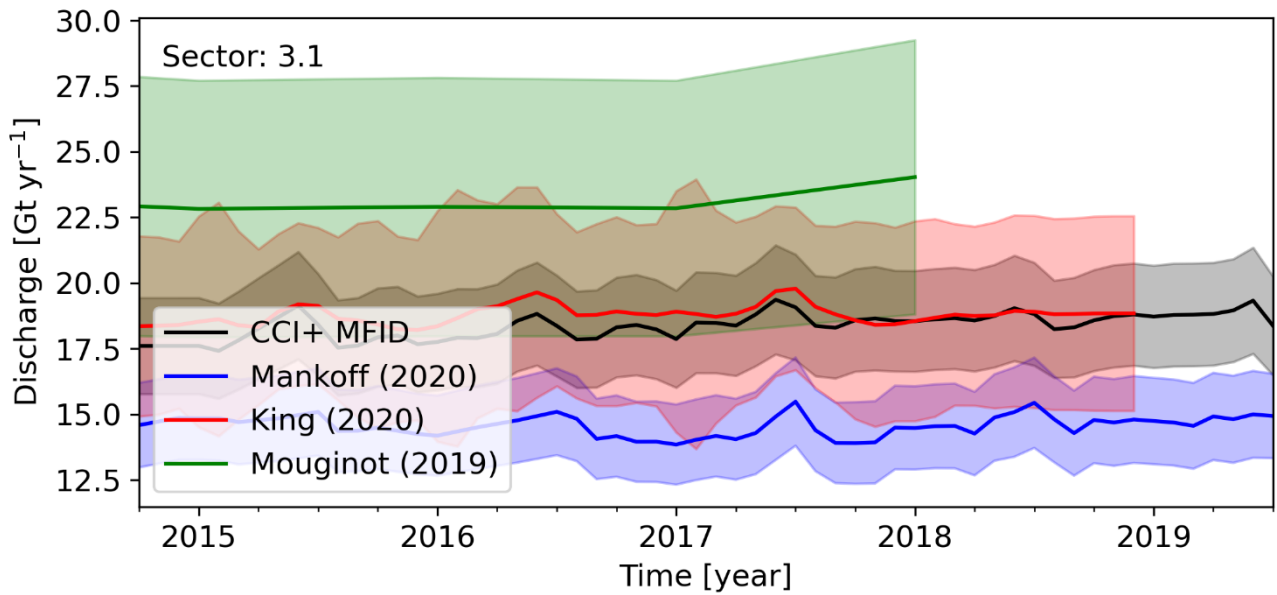


Figure 5-5: Same as Figure 5-1 caption.

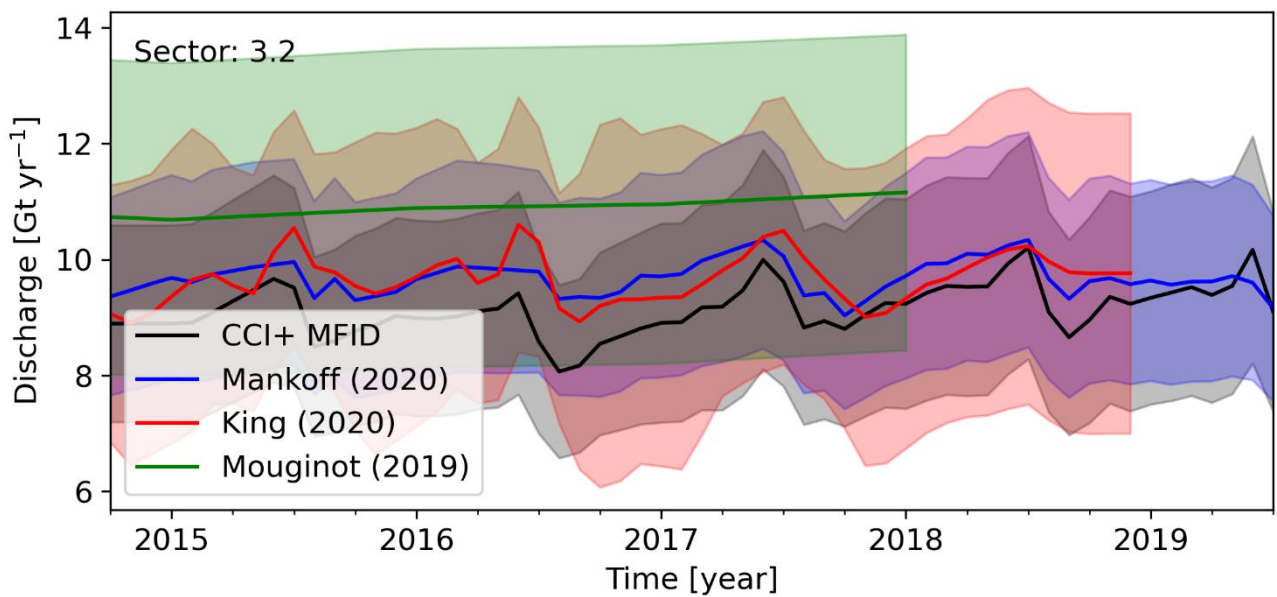


Figure 5-6: Same as Figure 5-1 caption.

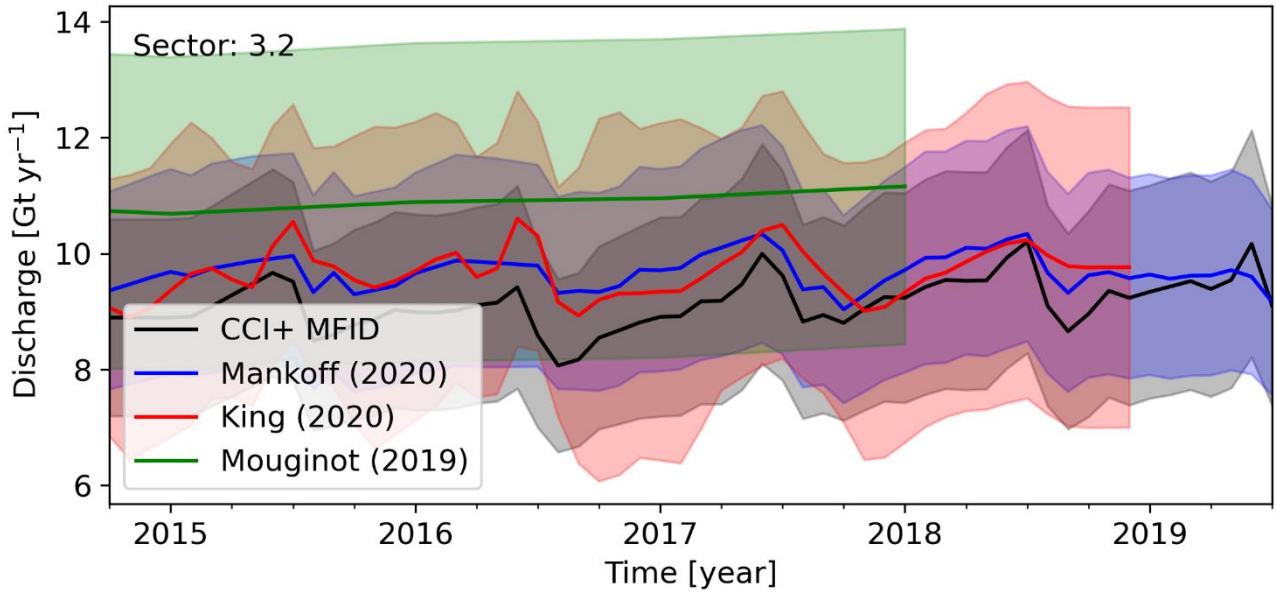


Figure 5-7: Same as Figure 5-1 caption.

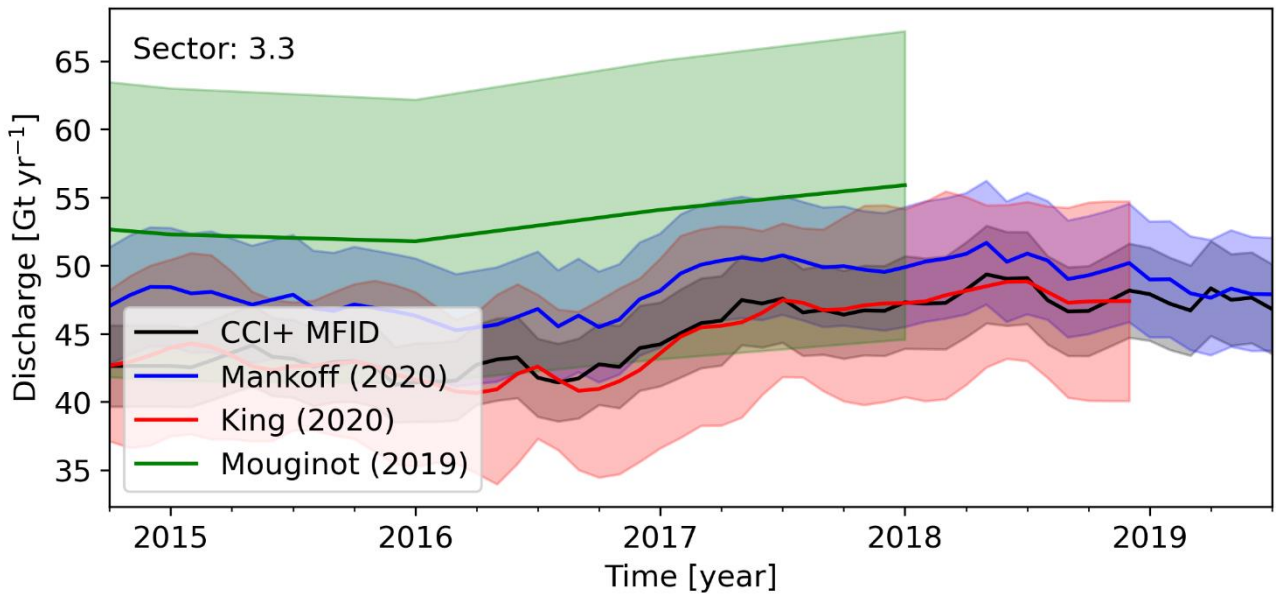


Figure 5-8: Same as Figure 5-1 caption.

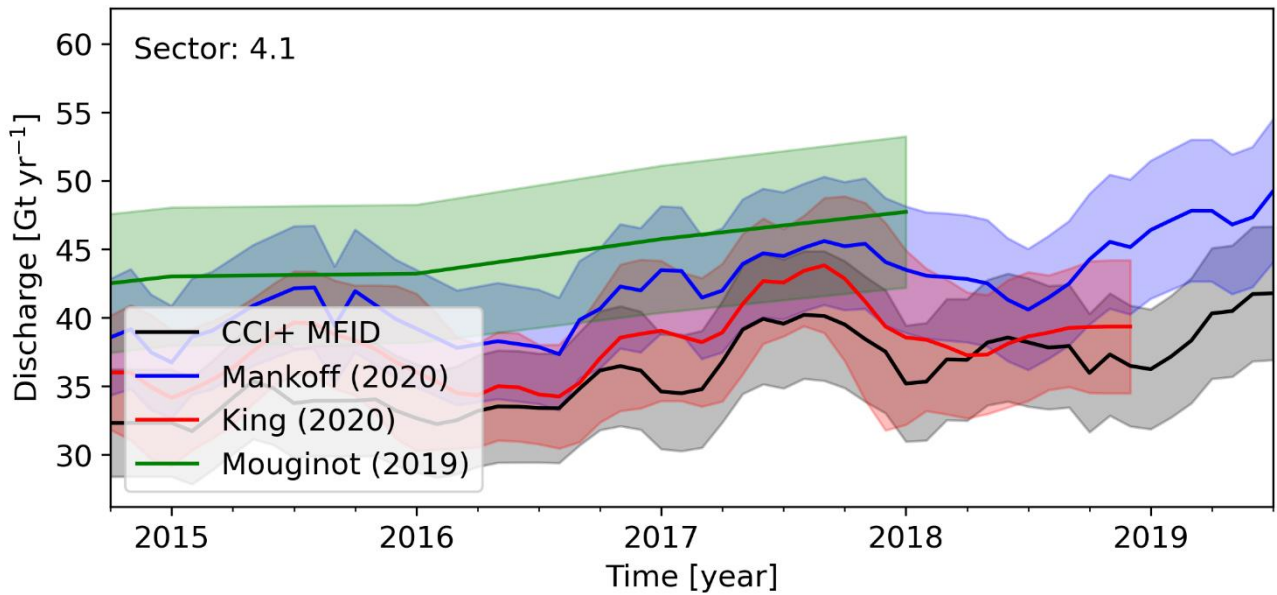


Figure 5-9: Same as Figure 5-1 caption.

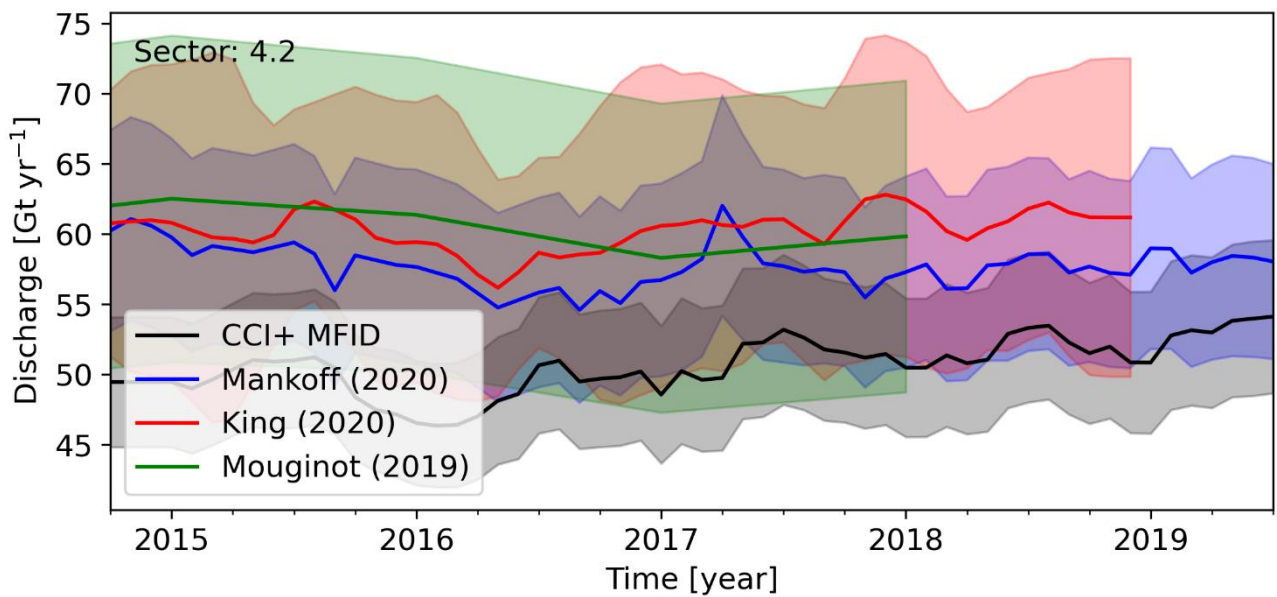


Figure 5-10: Same as Figure 5-1 caption.

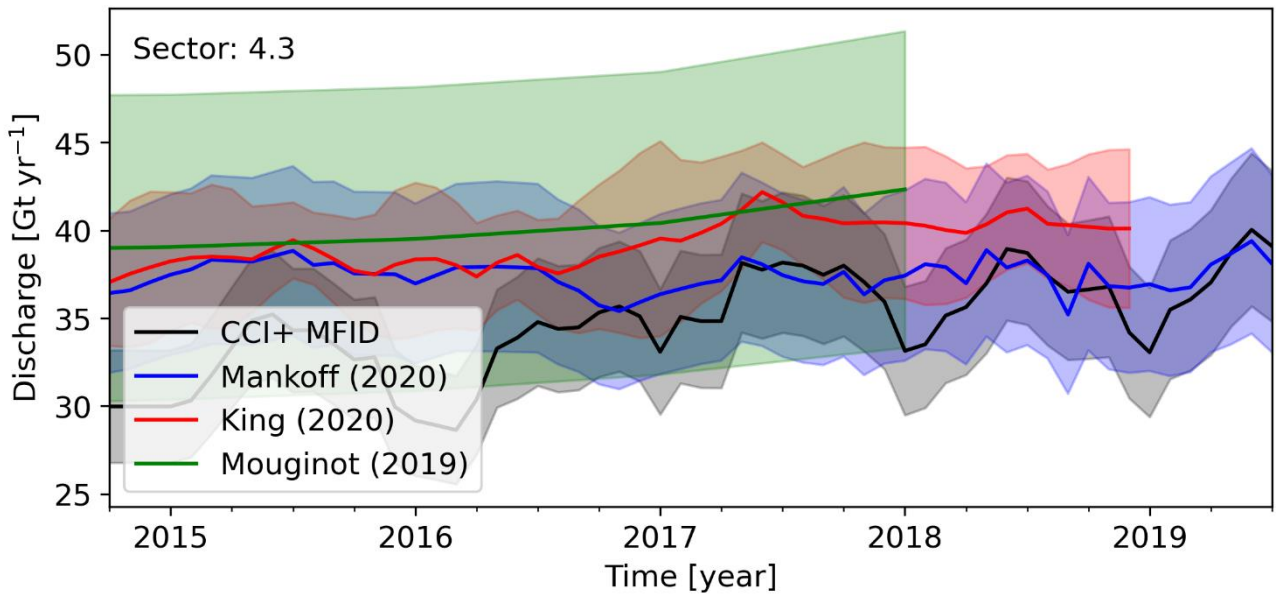


Figure 5-11: Same as Figure 5-1 caption.

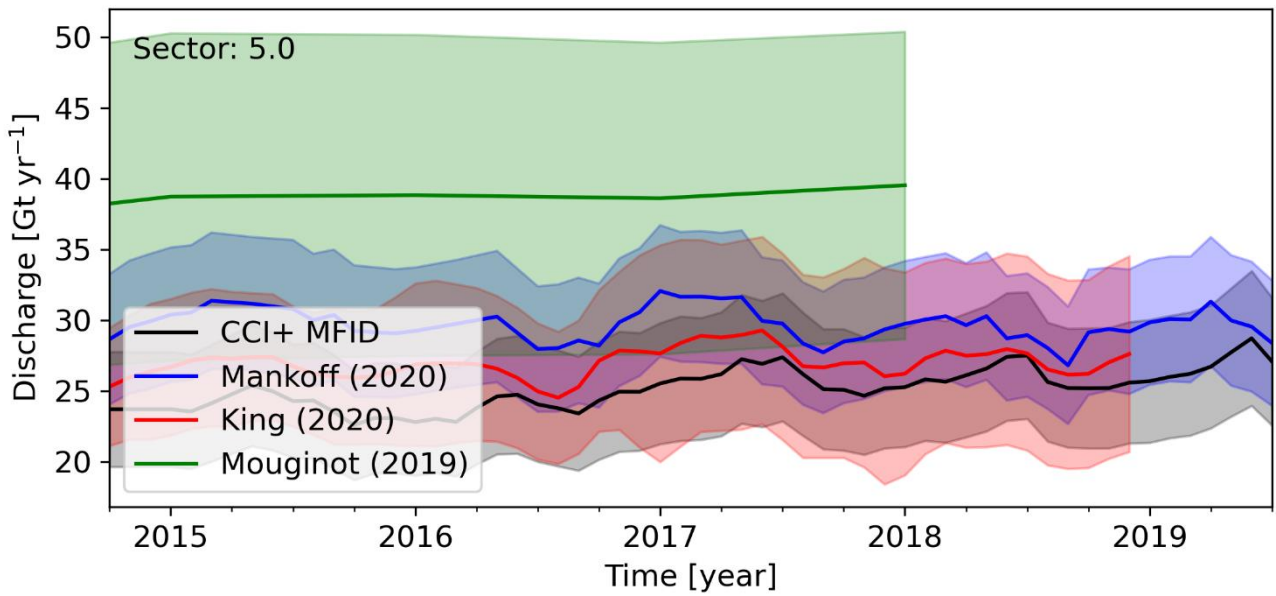


Figure 5-12: Same as Figure 5-1 caption.

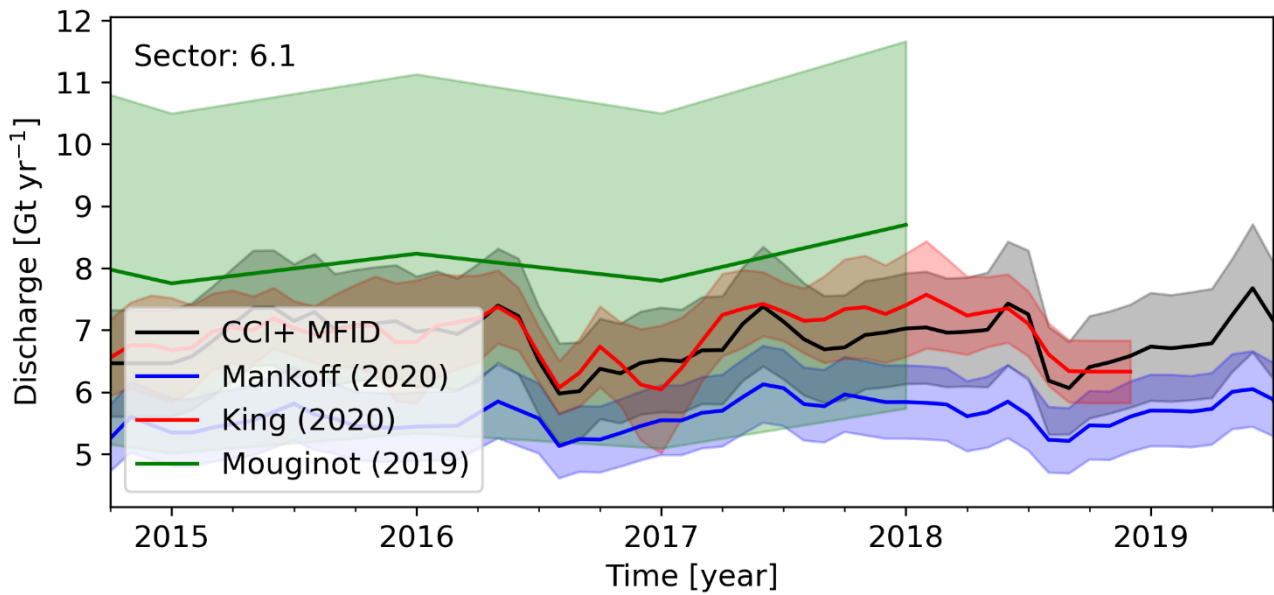


Figure 5-13: Same as Figure 5-1 caption.

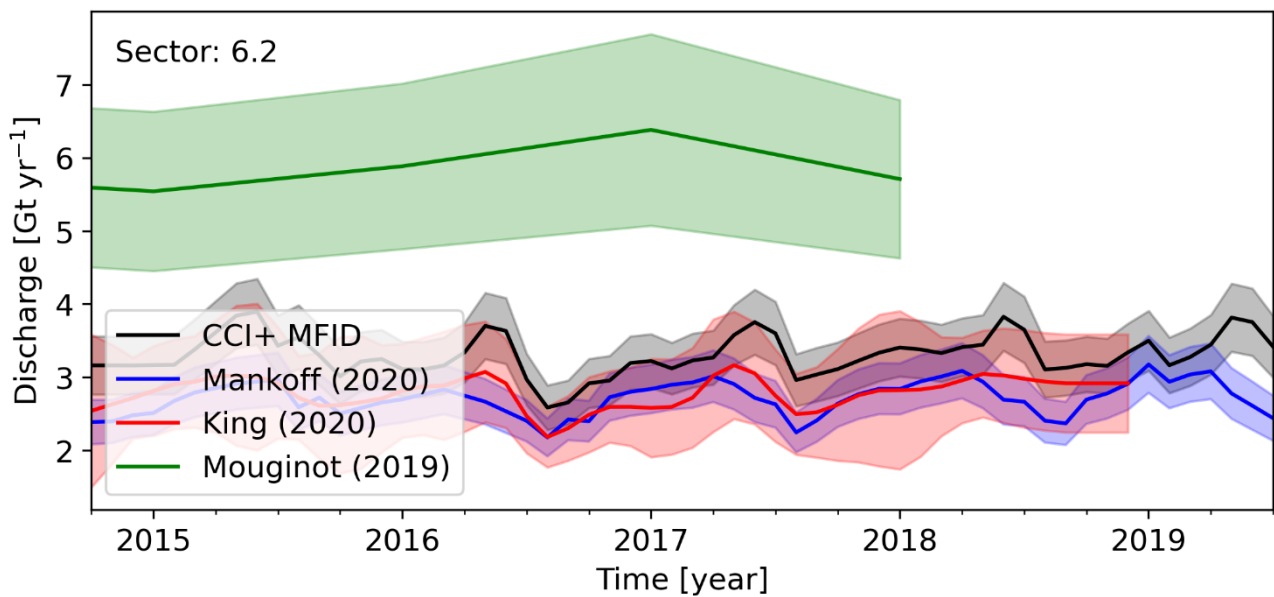


Figure 5-14: Same as Figure 5-1 caption.

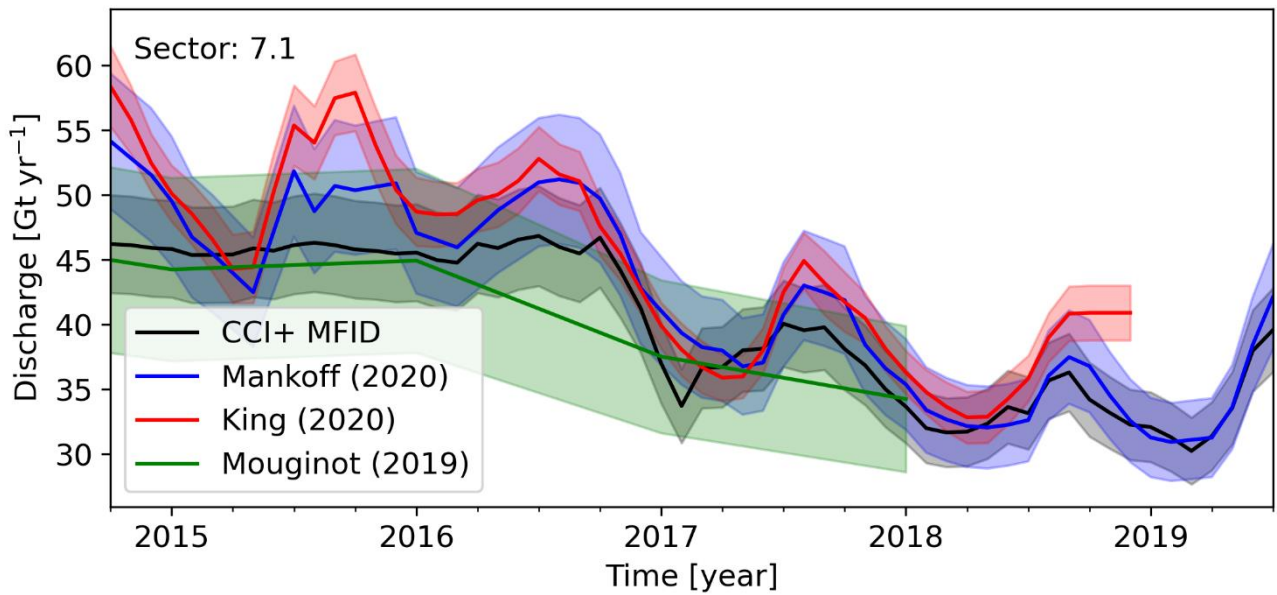


Figure 5-15: Same as Figure 5-1 caption.

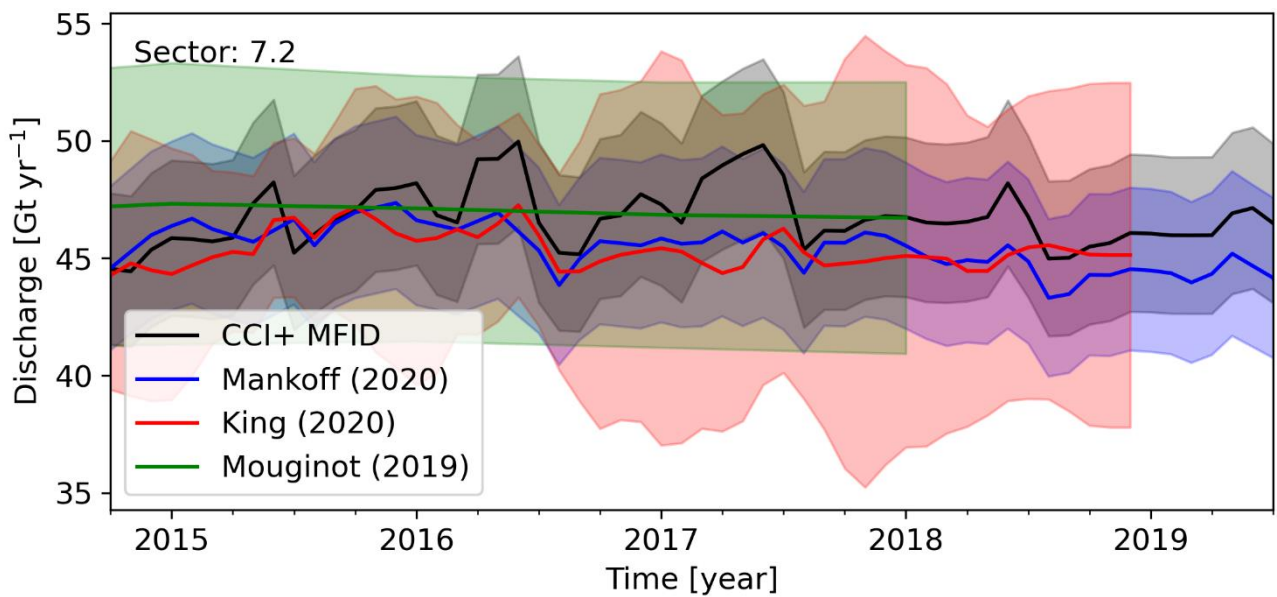


Figure 5-16: Same as Figure 5-1 caption.

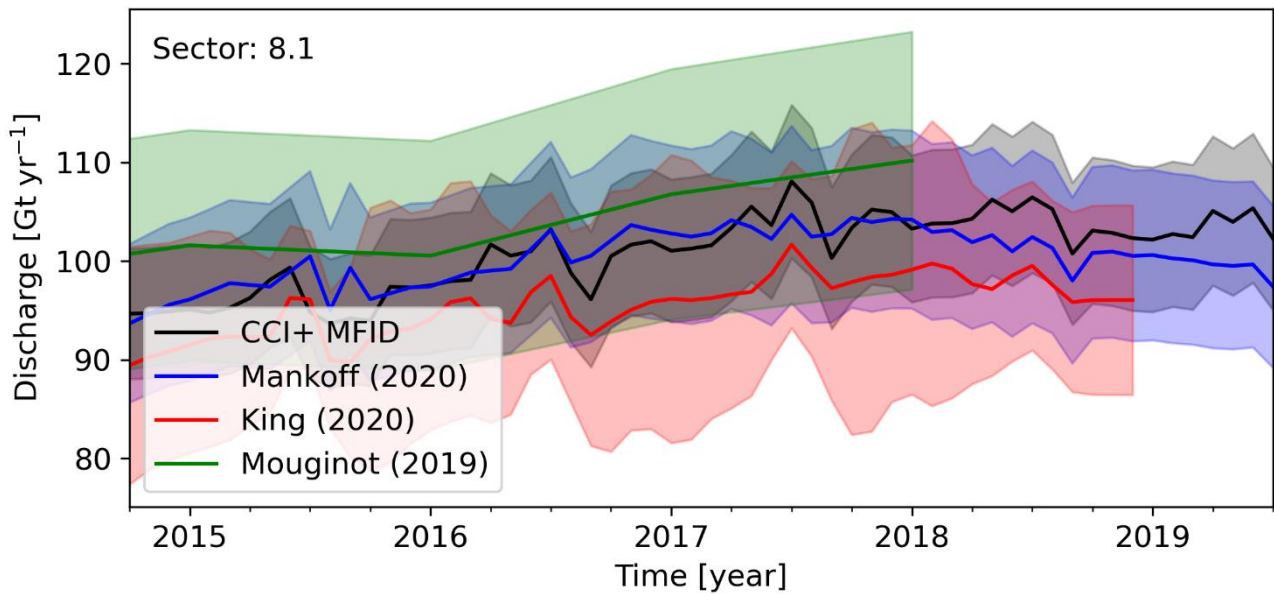


Figure 5-17: Same as Figure 5-1 caption.

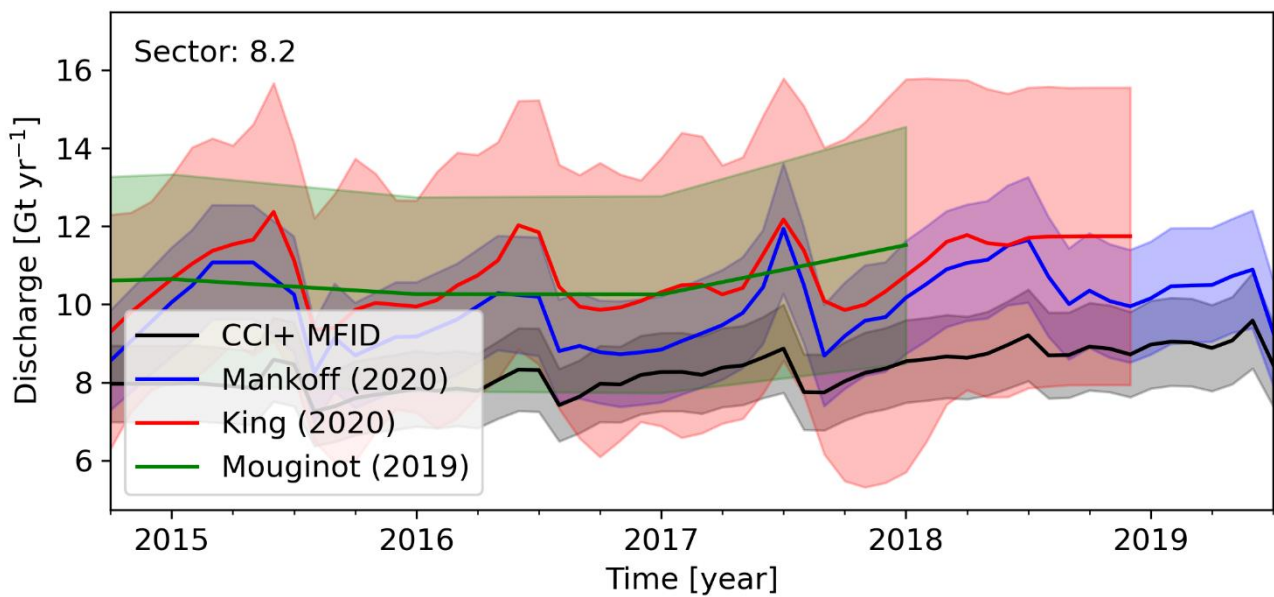


Figure 5-18: Same as Figure 5-1 caption.

## 6 Supraglacial Lakes

Supraglacial lakes (SGLs) have been identified in the catchment of Sermeq Kujalleq (SK, also known as Jakobshavn Isbræ) for the melt season of 2019. The selected catchment area covers 160,039.11 km<sup>2</sup>, approximately 22% of SK's catchment. Supraglacial lakes were detected in this area for each available time step, subject to data availability and cloud cover. Over 6000 ( $\pm 15\%$ ) lake features were identified over the melt season, with an average lake area of 0.4 km<sup>2</sup> ( $\pm 22\%$ ). As expected, a high majority of these lakes were identified in the lower part of the SK catchment (3190 lakes in total), with the maximum number of lakes evident during the peak of the melt season in August.

Although SGL is not a standard data product in the Greenland Ice Sheet CCI+ project, it is recognised that it is an important R&D product because glacier dynamics are understood to be inherently linked to supraglacial lake extent and drainage (e.g. Das et al., 2008; Andrews et al., 2018). As a result, validation analysis of the SGLs is essential to this work.

The validation analysis could be conducted under two approaches:

1. Through inter-comparison with available independent datasets for the same study area
2. Through inter-comparison with alternative sensors for the same time period; hereafter referred to as the sensor inter-comparison

Many remote sensing studies have previously been conducted at SK to derive supraglacial lakes, including those derived from MODIS, Landsat, Sentinel-2, and WorldView imagery (Hoffman et al., 2011; Liang et al. 2012; Williamson et al., 2017; Rowley et al., 2019). However, no ideal supraglacial lake dataset was found that was suitable for comparison to the dataset derived here, either due to spatial (e.g. Rowley et al., 2019) or temporal (Liang et al., 2012) mismatches. For this reason, we focus on the latter approach for our validation analysis – sensor inter-comparison.

### 6.1 Sources and selection of independent validation data

Landsat-8 imagery is used for the sensor inter-comparison, adopting the detection method used for the SGL product to derive supraglacial water bodies from coinciding Landsat-8 scenes. Scenes were selected based on three key criteria: 1) cloud cover (less than 60%); 2) spatial coverage (across the entire monitoring area used for the SGL product); and 3) corresponding with Sentinel-2 image acquisitions (less than 24 hours). The selected scenes are outlined in Table 6-1.

**Table 6-1: Selected Landsat-8 scenes as validation data.**

Scene IDs	Acquisition date	Cloud cover	Corresponding SGL time step for comparison
LC08_L1TP_008011_20190507_20190521_01_T1 LC08_L1TP_008012_20190507_20190521_01_T1	07/05/2019	10% 17%	06/05/2019
LC08_L1TP_008011_20190523_20190604_01_T1 LC08_L1TP_008012_20190523_20190604_01_T1	23/05/2019	0% 21%	22/05/2019 & 24/05/2019 (average)
LC08_L1TP_082233_20190530_20190605_01_T1 LC08_L1TP_009011_20190530_20190605_01_T1	30/05/2019	3% 3%	30/05/2019
LC08_L1TP_008011_20190608_20190619_01_T1 LC08_L1TP_008012_20190608_20190619_01_T1	08/06/2019	1% 55%	08/06/2019
LC08_L1TP_008011_20190811_20190820_01_T1 LC08_L1TP_008012_20190811_20190820_01_T1	11/08/2019	2% 7%	11/08/2019
LC08_L1TP_008011_20190827_20190903_01_T1 LC08_L1TP_008012_20190827_20190903_01_T1	27/08/2019	3% 23%	27/08/2019

## 6.2 Validation procedure

The Landsat-8 scenes outlined in Table 6-1 were processed in the same manner as described for the SGL product – a dual threshold was applied to create binary rasters from NDWI images, which were subsequently vectorised and filtered using a DEM mask denoting sinks in the ice surface. This method is adopted from those provided by Yang and Smith (2013) and Yang (2019), modified for batch processing and specific file handling procedures compatible with the ESA CCI+ product specifications.

Statistics were generated from the resulting supraglacial water bodies, including lake abundance, total lake area and average lake area. These statistics were compared to those determined from the SGL product. Additionally, individual examples of supraglacial lakes were selected and compared to provide further insight into the sensor inter-comparison.

## 6.3 Validation procedure outcome

Generally, Sentinel-2 detected more lakes than Landsat-8, with an average difference of 34 lakes per time step. This is likely due to differing coverage due to scene cover and cloud cover but could also be linked to the difference in spatial resolution which is commonly observed in inter-comparison studies (Williamson et al., 2018).

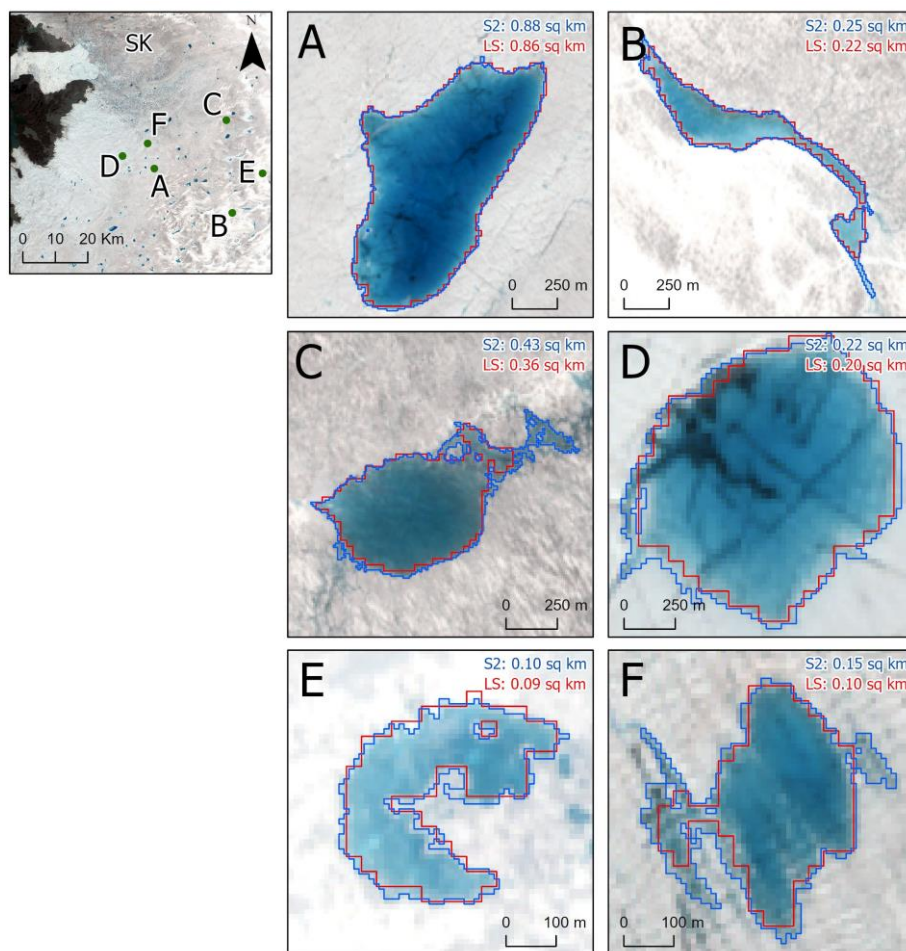


Figure 6-1: Selected lakes from the sensor inter-comparison analysis. Lakes are taken from the supraglacial lake datasets derived from Sentinel-2 and Landsat-8 scenes acquired on 08/06/2019. Zoom-ins of the Sentinel-2 subset (left) shown examples of lake delineation with unconstrained lake forms (A, D), intricate or constrained forms (B, E, F) and more challenging forms that include saturated snow (C).

Comparison between the SGL and the Landsat-derived supraglacial water bodies indicate slight discrepancies in individual lake form, with an average difference in lake size of 0.03 km<sup>2</sup> (8%). This forms an RMSE of 0.159 km<sup>2</sup>. The examples in Fig. 6-1 demonstrate differences in form between supraglacial water bodies derived from Sentinel-2 and Landsat-8 imagery acquired 30/05/2019, with both closely corresponding delineations (e.g. A, D) and relatively poor delineations (e.g. C, F). Discrepancies in lake area appear to generally stem from the difference in spatial resolution, where lake areas are underestimated from the 30-m resolution Landsat-8 imagery compared to the 10-m resolution Sentinel-2 imagery. This is especially evident when lake forms have intricate forms or include areas of saturated snow, which are not as distinguished in the Landsat-8 imagery (e.g. E and F).

## 6.4 Recommendations for products improvement

Overall, the sensor inter-comparison validation shows good correspondence between the SGL and lakes derived from Landsat-8 imagery, with an average difference in lake size of 0.03 km<sup>2</sup> (8%) and an RMSE of 0.159 km<sup>2</sup>. Selected examples demonstrate that this difference largely reflects the difference in spatial resolution between Sentinel-2 and Landsat-8.

A recommendation to improve the SGL in future work would be to detect supraglacial water bodies from both sensors, and other available optical imagery, to form a multi-sensor approach. By doing this, the temporal resolution of the SGL dataset could be improved, and coinciding scene acquisitions could be used to form a robust validation approach as demonstrated in this report.

Through undertaking this validation analysis, the processing chain for generating the SGL dataset was easily modified to incorporate the inclusion of Landsat-8 imagery alongside Sentinel-2, proving that this recommendation is an achievable goal that is already implemented in processing chains for future work.

## 7 References

- Andrews, L. C. et al. (2018) Seasonal evolution of the subglacial hydrologic system modified by supraglacial lake drainage in Western Greenland. *Journal of Geophysical Research: Earth Surface* **123**, 1479-1496. 10.1029/2017JF004585
- Blair, B. and Hofton, M.: IceBridge LVIS L2 Geolocated Surface Elevation Product. Boulder, Colorado USA: NASA DAAC at the National Snow and Ice Data Center. <http://nsidc.org/data/docs/daac/icebridge/ilvis2/>, 2012.
- Brenner, A. C., Bindschadler, R. A., Thomas, R. H. and Zwally, H. J.: Slope-induced errors in radar altimetry over continental ice sheets, *J. Geophys. Res. - Oceans*, vol. 88, no.C3, pp. 1617–1623, 1983.
- Das, S.B. et al. (2008) Fracture propagation to the base of the Greenland Ice Sheet during supraglacial lake drainage. *Science* **320**, 778-781. 10.1126/science.1153360
- Fausto, R.S. and van As, D. 2019. Programme for monitoring of the Greenland ice sheet (PROMICE): Automatic weather station data. Version: v03, Dataset published via Geological Survey of Denmark and Greenland. doi: <https://doi.org/10.22008/promice/data/aws>
- Forsberg, R., Sørensen, L. & Simonsen, S: Greenland and Antarctica Ice Sheet Mass Changes and Effects on Global Sea Level. *Surveys in Geophysics* (2017) 38: 89. doi:10.1007/s10712-016-9398-7
- Geological Survey of Denmark and Greenland: PROMICE, Programme for Monitoring of the Greenland Ice Sheet. <http://www.promice.org/home.html>, 2015.
- Groh, A.; Horwath, M.; Horvath, A.; Meister, R.; Sørensen, L.S.; Barletta, V.R.; Forsberg, R.; Wouters, B.; Ditmar, P.; Ran, J.; Klees, R.; Su, X.; Shang, K.; Guo, J.; Shum, C.K.; Schrama, E.; Shepherd, A. Evaluating GRACE Mass Change Time Series for the Antarctic and Greenland Ice Sheet-Methods and Results. *Geosciences* (2019), 9, 415. doi:10.3390/geosciences9100415.
- Hoffman, M.J. et al. (2011) Links between acceleration, melting, and supraglacial lake drainage of the western Greenland Ice Sheet. *Journal of Geophysical Research: Earth Surface* **116**, F4, F04035. 10.1029/2010JF001934
- Hvidberg, C.S., et al., User Requirements Document for the Ice\_Sheets\_cci project of ESA's Climate Change Initiative, version 1.5, 03 Aug 2012. Available from: <http://www.esa-icesheets-cci.org/>
- Joughin, I. 2002. Ice-sheet velocity mapping: a combined interferometric and speckle-tracking approach. *Annals of Glaciology*, 34, 195–201. <https://doi.org/10.3189/172756402781817978>
- Joughin, I., B. Smith, I. Howat, and T. Scambos. 2015, updated 2018. MEaSURES Greenland Ice Sheet Velocity Map from InSAR Data, Version 2. [Indicate subset used]. Boulder, Colorado USA. NASA National Snow and Ice Data Center Distributed Active Archive Center. doi: <https://doi.org/10.5067/OC7B04ZM9G6Q> [Date Accessed: Date accessed: August 2020]
- Joughin, I., I. Howat, B. Smith, and T. Scambos. 2020. MEaSURES Greenland Ice Velocity: Selected Glacier Site Velocity Maps from InSAR, Version 3. [Indicate subset used]. Boulder, Colorado USA. NASA National Snow and Ice Data Center Distributed Active Archive Center. doi: <https://doi.org/10.5067/YXMJRME5OUNC> [Date accessed: August 2020]
- Khvorostovsky, K.: Merging and analysis of elevation time series over Greenland ice sheet from satellite radar altimetry, *IEEE Trans. Geosc. Remote Sens.*, 50, 1:23–36. doi: 10.1109/TGRS.2011.2160071, 2012.
- King, Michalea D., Howat, Ian M., Jeong, Seongsu, Noh, Myoung J., Wouters, Bert, Noël, Brice, van den Broeke, Michiel R.: Seasonal to decadal variability in ice discharge from the Greenland Ice Sheet, *The Cryosphere* 12(12), Copernicus GmbH, 3813–3825, 12 2018
- King, Michalea D., Howat, Ian M., Candela, Salvatore G., Noh, Myoung J., Jeong, Seongsu, Noël, Brice P. Y., van den Broeke, Michiel R., Wouters, Bert, Negrete, Adelaide: Dynamic ice loss from the Greenland Ice Sheet driven by sustained glacier retreat, *Communications Earth & Environment* 1(1), Springer Science and Business Media LLC, 8 2020
- Krabill, W. B.: IceBridge Level-4 ATM Surface Elevation Rate of Change. Boulder, Colorado USA: NASA DAAC at the National Snow and Ice Data Center. <http://nsidc.org/data/idhdt4.html>, 2014.

- Krabill, W. B.: IceBridge ATM L1B Elevation and Return Strength. Boulder, Colorado USA: NASA DAAC at the National Snow and Ice Data Center. <http://nsidc.org/data/ilatm1b.html>, 2010.
- Krabill, W. B., Abdalati, W., Frederick, E., Manizade, S., Martin, C., Sonntag, J., Swift, R., Thomas, R. and J. Yungel, J.: Aircraft laser altimetry measurement of elevation changes of the Greenland Ice Sheet: technique and accuracy assessment, *J. Geodyn.*, 34:357–376. doi: 10.1016/S0264-3707(02)00040-6, 2002.
- Legresy, B., Papa, F., Remy, F., Vinay, G., van den Bosch, M. and Zanife, O.-Z.: ENVISAT radar altimeter measurements over continental surfaces and ice caps using the ICE-2 retracking algorithm, *Remote Sens. Environ.*, 95(2):150–163. doi: 10.1016/j.rse.2004.11.018, 2005.
- Liang, Y.-L. et al. (2012) A decadal investigation of supraglacial lakes in West Greenland using a fully automatic detection and tracking algorithm. *Remote Sensing of Environment* **123**, 127-138. 10.1016/j.rse.2012.03.020
- McMillan, M., Muir, A., Shepherd, A., Escolà, R., Roca, M., Aublanc, J., Thibaut, P., Restano, M., Ambrozio, A., and Benveniste, J.: Sentinel-3 Delay-Doppler altimetry over Antarctica, *The Cryosphere*, 13, 709–722, <https://doi.org/10.5194/tc-13-709-2019>, 2019.
- Mankoff, Kenneth D., Solgaard, Anne, Colgan, William, Ahlstrøm, Andreas P., Khan, Shfaqat Abbas, Fausto, Robert S.: Greenland Ice Sheet solid ice discharge from 1986 through March 2020, *Earth System Science Data* 12(2), Copernicus GmbH, 1367–1383, 6 2020
- Mouginot, Jérémie, Rignot, Eric, Bjørk, Anders A., van den Broeke, Michiel, Millan, Romain, Morlighem, Mathieu, Noël, Brice, Scheuchl, Bernd, Wood, Michael: Forty-six years of Greenland Ice Sheet mass balance from 1972 to 2018, *Proceedings of the National Academy of Sciences*, *Proceedings of the National Academy of Sciences*, 201904242, 4 2019
- Rastner, P., Bolch, T., Mölg, N., Machguth, H., Le Bris, R., Paul, F. 2012, updated 2018. The first complete inventory of the local glaciers and ice caps on Greenland. *The Cryosphere*, 6, 1483-1495. doi:10.5194/tc-6-1483-2012
- Roemer, S., Legresy, B., Horwath, M., and Dietrich, R.: Refined analysis of radar altimetry data applied to the region of the subglacial Lake Vostok/Antarctica, *Remote Sens. Environ.*, vol. 106, no. 3, pp. 269–284, 2007.
- Rowley, N.A. & Fegyveresi, J.M. (2019) Generating a supraglacial melt-lake inventory near Jakobshavn, West Greenland, using a new semi-automated lake-mapping technique. *Polar Geography* **42:2**, 89-108. 10.1080/1088937X.2019.1578289
- Shepherd, A., Ivins, E. R., Geruo, A., Barletta, V. R., Bentley, M. J., Bettadpur, S., ... & Horwath, M. (2012). A reconciled estimate of ice-sheet mass balance. *Science*, 338(6111), 1183-1189.
- Shepherd, A., Ivins, E., Rignot, E. et al. Mass balance of the Antarctic Ice Sheet from 1992 to 2017. *Nature* 558, 219–222 (2018). <https://doi.org/10.1038/s41586-018-0179-y>
- Shepherd, A., Ivins, E., Rignot, E. et al. Mass balance of the Greenland Ice Sheet from 1992 to 2018. *Nature* 579, 233–239 (2020). <https://doi.org/10.1038/s41586-019-1855-2>
- Simonsen, S. B. and Sørensen, L. S. (2017): Implications of changing scattering properties on Greenland ice sheet volume change from Cryosat-2 altimetry. *Remote Sensing of Environment*, 190, p. 207-216, 2017.
- Skourup, H., Barletta, V., Einarsson, I., Forsberg, R., Haas, C., Helm, V., Hendricks, S., Hvidegaard, S. M., and Sørensen, L. S.: ESA CryoVEx 2011: Airborne field campaign with ASIRAS radar, EM induction sounder and laser scanner. DTU Space, National Space Institute, Technical University of Denmark, 1st edition, 2011.
- Slater T., A. Shepherd, M. Mcmillan, T. W. K. Armitage, I. Otosaka and R. J. Arthern, "Compensating Changes in the Penetration Depth of Pulse-Limited Radar Altimetry Over the Greenland Ice Sheet," in *IEEE Transactions on Geoscience and Remote Sensing*, vol. 57, no. 12, pp. 9633-9642, Dec. 2019, doi: 10.1109/TGRS.2019.2928232.



Sørensen, L. S., Simonsen, S. B., Forsberg, R., Stenseng, L., Skourup, H., Kristensen, S. S., & Colgan, W. (2017). Circum-Greenland, ice-thickness measurements collected during PROMICE airborne surveys in 2007, 2011 and 2015. *Geological Survey of Denmark and Greenland Bulletin*, 79-82.

Williamson, A.G. et al. (2017) A Fully Automated Supraglacial lake area and volume Tracking ("FAST") algorithm: Development and application using MODIS imagery of West Greenland. *Remote Sensing of Environment* **196**, 113-133. 10.1016/j.rse.2017.04.032

Yang, K. & Smith, L. (2013) Supraglacial streams on the Greenland Ice Sheet delineated from combined spectral-shape information in high-resolution satellite imagery. *IEEE Geosci. Remote Sens. Lett.*, 10 (4), 801- 805.

Yang, K. (2019) Supraglacial river and lake analysis [software]. *figshare*. 10.6084/m9.figshare.9758051.v1.

Zwally, H. Jay, Giovinetto, Mario B., Beckley, Matthew A., Saba, Jack L.: Antarctic and Greenland Drainage Systems, 2012, GSFC Cryospheric Sciences Laboratory